Cell

Discovery of a Class of Endogenous Mammalian Lipids with Anti-Diabetic and Anti-inflammatory Effects

Mark M. Yore,[1,5] Ismail Syed,[1,5] Pedro M. Moraes-Vieira,[1] Tejia Zhang,[3,7] Mark A. Herman,[1] Edwin A. Homan,[3] Rajesh T. Patel,[2] Jennifer Lee,[1] Shili Chen,[3,7] Odile D. Peroni,[1] Abha S. Dhaneshwar,[1] Ann Hammarstedt,[4] Ulf Smith,[4] Timothy E. McGraw,[2] Alan Saghatelian,[3,6,7,*] and Barbara B. Kahn[1,6,*]

[1]Division of Endocrinology, Diabetes and Metabolism, Department of Medicine, Beth Israel Deaconess Medical Center and Harvard Medical School, Boston, MA 02215, USA

[2]Department of Biochemistry, Weill Cornell Medical College, New York, NY 10065, USA

[3]Department of Chemistry and Chemical Biology, Harvard University, Cambridge, MA 02138, USA

[4]Department of Molecular and Clinical Medicine, the Sahlgrenska Academy, University of Gothenburg, Gothenburg 41345, Sweden

[5]Co-first author

[6]Co-senior author

[7]Present address: Salk Institute for Biological Studies, Torrey Pines Road, La Jolla, CA 92037

*Correspondence: asaghatelian@salk.edu (A.S.), bkahn@bidmc.harvard.edu (B.B.K.)

http://dx.doi.org/10.1016/j.cell.2014.09.035

SUMMARY

Increased adipose tissue lipogenesis is associated with enhanced insulin sensitivity. Mice overexpressing the Glut4 glucose transporter in adipocytes have elevated lipogenesis and increased glucose tolerance despite being obese with elevated circulating fatty acids. Lipidomic analysis of adipose tissue revealed the existence of branched *f*atty *a*cid esters of *h*ydroxy *f*atty *a*cids (FAHFAs) that were elevated 16- to 18-fold in these mice. FAHFA isomers differ by the branched ester position on the hydroxy fatty acid (e.g., *p*almitic-*a*cid-9-*h*ydroxy-stearic-*a*cid, 9-PAHSA). PAHSAs are synthesized in vivo and regulated by fasting and high-fat feeding. PAHSA levels correlate highly with insulin sensitivity and are reduced in adipose tissue and serum of insulin-resistant humans. PAHSA administration in mice lowers ambient glycemia and improves glucose tolerance while stimulating GLP-1 and insulin secretion. PAHSAs also reduce adipose tissue inflammation. In adipocytes, PAHSAs signal through GPR120 to enhance insulin-stimulated glucose uptake. Thus, FAHFAs are endogenous lipids with the potential to treat type 2 diabetes.

INTRODUCTION

Obesity and type 2 diabetes (T2D) are at epidemic proportions worldwide (Hu, 2011). The major pathogenic factors underlying T2D are resistance to insulin action in peripheral tissues and dysregulated insulin secretion. The Glut4 glucose transporter is the major insulin-regulated glucose transporter and mediates glucose uptake into skeletal muscle, heart, and adipocytes in response to rising insulin after a meal (Shepherd and Kahn, 1999). In humans and rodents with obesity or T2D, Glut4 is downregulated selectively in adipose tissue (AT) and not in muscle (Shepherd and Kahn, 1999). This alters AT biology leading to systemic insulin resistance (Abel et al., 2001). Glut4 knockdown selectively in adipocytes in mice results in insulin resistance and increased T2D risk (Abel et al., 2001), whereas adipose-selective overexpression of Glut4 (AG4OX) lowers fasting glycemia and enhances glucose tolerance (Carvalho et al., 2005; Shepherd et al., 1993). These effects in AG4OX mice are mediated by glucose-dependent induction of lipogenesis in AT driven by ChREBP (Herman et al., 2012), a transcription factor that regulates both glycolysis and lipogenesis (Iizuka et al., 2004; Ma et al., 2005). ChREBP knockout in AG4OX mice completely reverses the enhanced glucose tolerance (Herman et al., 2012). Expression of ChREBP and lipogenic genes in AT is highly associated with insulin sensitivity in humans and rodents (Herman et al., 2012; Roberts et al., 2009) and increased de novo lipogenesis in AT has favorable metabolic effects including potentially increasing longevity (Bruss et al., 2010).

Elevated circulating fatty acids are generally associated with insulin resistance and glucose intolerance (Boden and Shulman, 2002). However, certain fatty acids such as dietary omega-3 fatty acids (Oh et al., 2010; Virtanen et al., 2014) and the endogenously produced palmitoleate (Cao et al., 2008) have favorable metabolic effects. Furthermore, large epidemiological studies show that an increased ratio of unsaturated to saturated fatty acids in serum triacylglycerols is associated with a reduced risk of T2D (Rhee et al., 2011; Risérus et al., 2009). Similarly, an increased ratio of monounsaturated to saturated fatty acids in the liver is associated with insulin sensitivity even with extensive hepatic steatosis (Benhamed et al., 2012). AG4OX mice have elevated circulating fatty acids and increased adiposity,

yet have lower fasting glycemia and profoundly enhanced glucose tolerance compared to controls (Carvalho et al., 2005; Herman et al., 2012; Shepherd et al., 1993). This raised the possibility that enhanced AT lipogenesis in response to Glut4 overexpression might drive the production of lipids which have favorable metabolic effects. Since Glut4 (Carvalho et al., 2005; Shepherd and Kahn, 1999) and ChREBP (Herman et al., 2012) expression are downregulated in AT in insulin-resistant humans and rodents, the production of these metabolically favorable lipids may be low in these states. To test these hypotheses, we performed lipidomic analysis of AT from wild-type (WT) and AG4OX mice.

RESULTS

Identification of a Class of Glut4-Regulated Lipids

Using a quantitative mass spectrometry (MS) lipidomics platform (Saghatelian et al., 2004), we detected more than 1,400 ions in AT, 6% of which had a 2- to 4-fold difference between AG4OX and WT mice. A cluster of ions in AG4OX AT was elevated $\geq$16-fold (Figure 1A). The measured accurate mass of these ions enabled us to calculate their molecular formulas as $C_{32}H_{61}O_4$ (509.4575), $C_{34}H_{63}O_4$ (535.4732), $C_{34}H_{65}O_4$ (537.4888), and $C_{36}H_{67}O_4$ (563.5045). These formulas all contain a unique signature of four oxygen atoms indicating that these ions are members of a single lipid class. These formulas do not correspond to any known metabolite in the Metlin (Smith et al., 2005) and Lipid Maps (Sud et al., 2007) metabolite databases. We hypothesized these lipids might contribute to glucose-insulin homeostasis because of their abundance in AG4OX mice, in which improved glucose tolerance depends on enhanced AT lipogenesis (Herman et al., 2012). Therefore, we proceeded to determine the molecular structures and biologic effects of these lipids.

The mass differences among these ions suggested they contain fatty acids. Fragmentation of the 537 ion generated several product ions with masses of 255, 281, and 299 (Figure 1B), which correspond to palmitic acid (PA), octadecenoic acid, and hydroxy-stearic acid (HSA), respectively. The molecular formula of the 537 ion ($C_{34}H_{65}O_4$) does not contain any double bonds. This indicates that octadecenoic acid, which contains a double bond, results from fragmentation in the MS and is not part of the natural metabolite. Based on the chemical formula and the fact that this metabolite ionized only in the negative mode, the most reasonable structure for the 537 ion is an ester that combines PA and HSA to yield *p*almitic *a*cid-*h*ydroxy *s*tearic *a*cid (PAHSA) (Figures 1B and 1C). Based on this structural model and the masses detected for the other elevated ions, their structures are: *p*almitic *a*cid-*h*ydroxy *p*almitic *a*cid (PAHPA, m/z 509), *o*leic *a*cid-*h*ydroxy *s*tearic *a*cid (OAHSA, m/z 563), and the 535 ion is a mixture of *p*almitoleic acid-*h*ydroxy *s*tearic *a*cid (POHSA), and *o*leic *a*cid-*h*ydroxy *p*almitic *a*cid (OAHPA) (Figure 1C). We refer to this class of natural-occurring lipids as *f*atty *a*cid-*h*ydroxy *f*atty *a*cids (Figures 1C and 1D), abbreviated as FAHFAs. An additional ion, detected in positive ionization mode, was also upregulated in AG4OX AT (Figure 1A) but the molecular formula indicated it is not a FAHFA, and therefore we did not characterize it further.

Using a targeted MS approach, we identified 16 FAHFA family members in mouse serum that consisted of four fatty acids and four hydroxy-fatty acids in different combinations (Figure 1D). FAHFAs with PO, PA, or OA as the fatty acid moiety and HPA or HSA as the hydroxy-fatty acid moiety were most highly increased in AG4OX compared to WT mice (Figure 1D). Because PAHSAs were the most highly upregulated family member in AT of AG4OX (Figure 1A), we investigated their biologic effects.

Tissue Distribution of Total PAHSAs in WT and AG4OX Mice and Regulation by ChREBP

Targeted MS revealed PAHSAs in all tissues analyzed. In WT mice, total PAHSA levels are highest in brown adipose tissue (BAT) followed by subcutaneous (SQ) white adipose tissue (WAT), perigonadal (PG) WAT, and liver (Figure 1E). Total PAHSA levels are very low in heart and gastrocnemius muscle (data not shown). PAHSA levels vary >7-fold among tissues in WT mice (Figure 1E). In WT serum, total PAHSA levels are ~7 nM (Figure 1E). In AG4OX mice, total PAHSA levels are 16- to 18-fold elevated in SQ and PG WAT, 3-fold in BAT and ~2-fold in serum compared to WT mice (Figure 1E). In contrast, PAHSA levels in liver of AG4OX mice are ~30% lower than WT. Thus, Glut4 overexpression in AT results in broad systemic regulation of PAHSAs with tissue-specific alterations.

Because ChREBP regulates AT lipogenesis in AG4OX, we tested whether ChREBP regulates PAHSA levels in vivo. ChREBP knockout in normal mice reduces total PAHSA levels ~75% in PG- and SQ-WAT with no change in serum (Figure 1F). Knocking out ChREBP in AG4OX completely reverses the marked elevation in PAHSA levels in PG- and SQ-WAT and serum.

Tissue Distribution of Specific PAHSA Isomers and Regulation in WT and AG4OX Mice

We observed multiple peaks in the chromatograms that correspond to different PAHSA isomers with the ester connected to a different carbon of the hydroxy-fatty acid resulting in a branched lipid. Fragmentation of PAHSAs from AT using high collisional energy tandem MS (Moe et al., 2004) produced two ions at 127 and 155 (Figure 1B) indicating that the ester is at the 9th carbon of the HSA (Figure 1C). We refer to this isomer as 9-PAHSA, which was confirmed by chemical synthesis and coelution with ^{13}C-9-PAHSA (Figure 2A). We also discovered PAHSAs with branched esters at carbons 5, 7, 8, 10, 11, 12, and 13 verified by comparison to synthetic standards (Figure 2A). Thus, there are at least eight PAHSA isomers. We achieved complete separation of all isomers except 13- and 12-PAHSA (Figure 2A), which we quantify together in all data sets.

We sought to determine which PAHSA isomers are upregulated in WAT and serum of AG4OX mice as an initial clue to which ones may have biologic activities that could affect glucose homeostasis. In WT serum, 13/12-, 11-, 10-, 9-, and 5-PAHSA are present at 0.4–2.5 nM, which is the range for signaling lipids such as prostacyclins, prostaglandins, steroids, and endocannabinoids. In WT WAT and BAT, 9-PAHSA is the most abundant isomer (Figure 2B). 13/12-, 11-, and 10-PAHSA are present at 20%–30% of 9-PAHSA levels and 8-, 7-, and 5-PAHSA are present at substantially lower concentrations (Figure 2B). Surprisingly, liver which is also a lipogenic tissue, has only

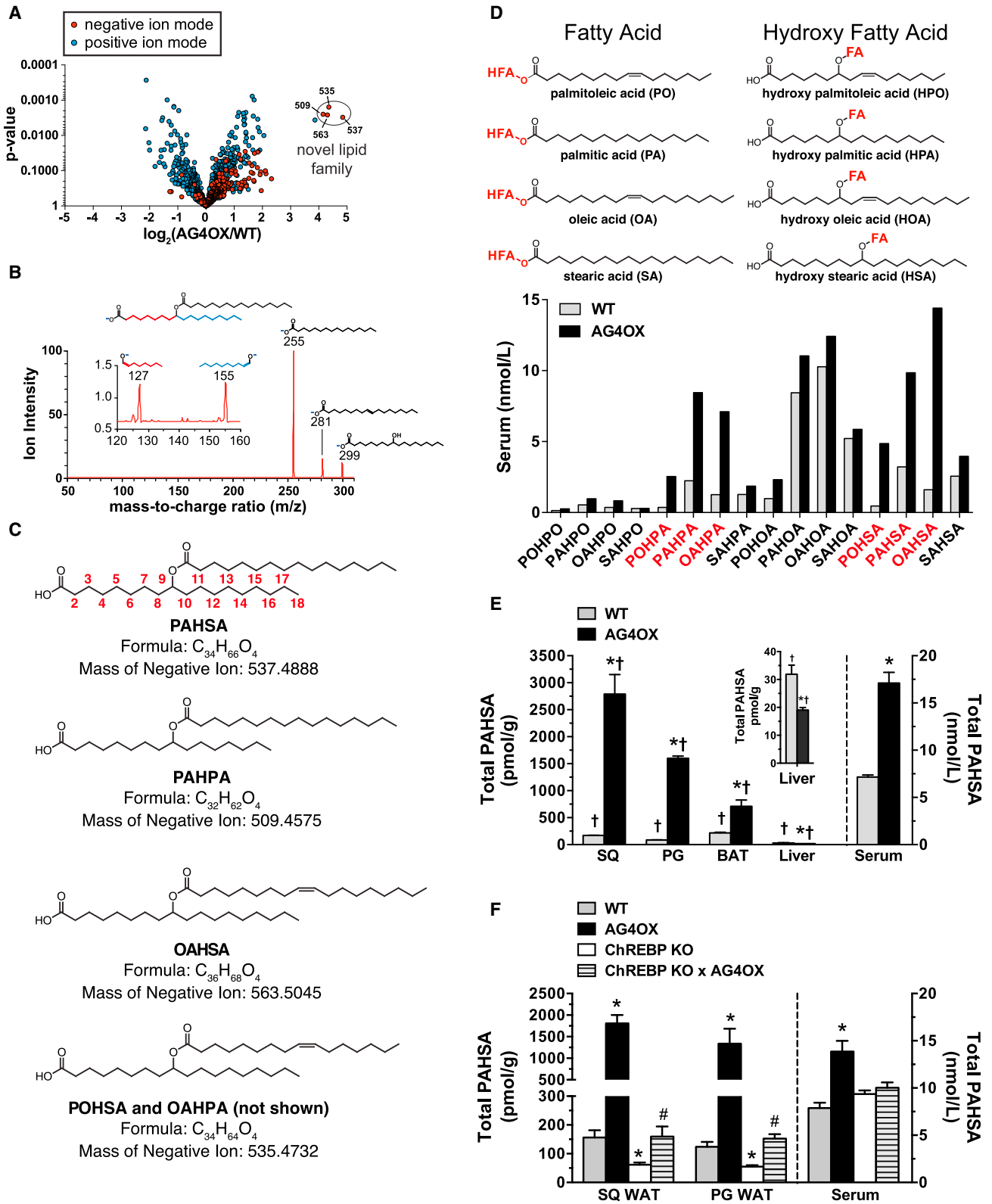

Figure 1. Discovery and Characterization of a Class of Lipids (FAHFAs)

(A) Comparative lipidomics of SQ white adipose tissue (WAT) from AG4OX and WT mice reveals the presence of a group of ions at m/z 509 (PAHPA), 535 (POHSA/OAHPA), 563 (OAHSA), and 537 (PAHSA) that are elevated 16- to 18-fold in AG4OX mice.

(legend continued on next page)

13/12- and 9-PAHSAs (Figure 2B). In AG4OX mice, all PAHSA isomers are elevated in serum, SQ and PG WAT and BAT with 9-PAHSA being the most highly upregulated. In contrast, in AG4OX liver, PAHSA isomers are reduced compared to WT. These data reveal that individual PAHSA isomers are coordinately upregulated in AG4OX WAT and BAT which may result from the effect of increased Glut4 to induce ChREBP and lipogenesis in these tissues (Herman et al., 2012; Tozzo et al., 1995). However, PAHSAs are reduced in AG4OX liver indicating tissue-specific mechanisms for regulating uptake, synthesis, degradation or release.

This is further indicated by the tissue distribution of specific PAHSA isomers in WT mice. 13/12- and 9-PAHSAs are present in all WT tissues examined (Figure 2C). 9-PAHSA is more abundant in AT than liver while 13/12-PAHSA is not. In contrast to 13/12- and 9-PAHSA, 5-PAHSA is restricted to AT, kidney, and serum (Figure 2C).

Physiologic Regulation of PAHSAs with Fasting

We examined PAHSA regulation with fasting (Figure 2D). In the fed state, total PAHSA levels are highest in BAT; slightly lower in SQ and PG WAT; and substantially lower in liver, pancreas, and kidney (Figure 2D). Fasting increases PAHSAs 2- to 3-fold in WAT and kidney and 65% in pancreas but does not alter the levels in BAT, liver, or serum (Figure 2D). Hence, PAHSAs undergo tissue-specific regulation with fasting (Figure 2D). The fasting-induced increase in PAHSAs in WAT is surprising since one would expect synthesis to be lower due to reduced lipogenesis and ChREBP with fasting. Indeed, in spite of elevated PAHSA levels, biosynthetic activity (described below) was not increased in WAT from fasted mice (data not shown). This may reflect inhibition of degradation or release. To better understand the mechanism, we determined fasting effects on PAHSA levels in AG4OX mice. Fasting further elevated PAHSAs in WAT but not in BAT or serum (Figure S1 available online). Since PAHSA levels in AG4OX WAT are regulated by ChREBP-driven lipogenesis (Figure 1E) and lipogenesis is not increased with fasting, these data demonstrate an additional level of regulation and support the possibility that fasting inhibits PAHSA degradation or release.

We also investigated regulation of individual PAHSA isomers with fasting (Figure 2E). Although total PAHSA levels are unchanged in serum of fasted mice (Figure 2D), specific isomers (10-, 9- and 5-PAHSA) are modestly decreased (Figure 2E). In SQ and PG WAT, most of the isomers (13/12-, 11-, 10-, 9-, and 8-PAHSA) including the more abundant ones are increased with fasting while 7- and 5-PAHSA are unchanged (Figure 2E). Fasting had no effect on any PAHSA isomer in BAT or liver while all isomers were upregulated in kidney. In pancreas, 11- and 9-PAHSA are increased with fasting while 13/12- and 7-PAHSA are unchanged. Thus, PAHSA isomer levels undergo tissue-specific and isomer-specific regulation with fasting (Figure 2E). The abundance of different PAHSA isomers in the fasted state differs by 60-fold in a given tissue (compare 9- with 5-PAHSA in SQ WAT) (Figure 2E). These results suggest that fasting regulates pathways involved in synthesis, degradation, and/or release of specific PAHSA isomers in a tissue- and isomer-specific manner.

Regulation of PAHSAs in Obesity and Insulin Resistance

We investigated PAHSA levels in insulin-resistant mice with high-fat-diet (HFD)-induced obesity (Figure 3A). After 9 weeks of HFD, mice were obese and diabetic (determined by GTT) (Figure S2A). HFD had differential effects on specific PAHSA isomers. 5- and 13/12-PAHSAs were downregulated in HFD mice in serum, PG and SQ WAT and BAT (Figure 3A) although the difference did not reach significance for 13/12-PAHSA in PG WAT. Strikingly, 10-, 9-, 8-, and 7-PAHSA were increased in PG WAT of HFD-fed mice. Most of these isomers were decreased in SQ WAT and BAT and unchanged in serum (Figure 3A). Total lipid ion signal measured in SQ WAT was unchanged between chow- and HFD-fed mice (Figure S2B). 13/12- and 9-PAHSA were also decreased in liver (Figure 3A). These studies demonstrate: (1) 5-PAHSA and 13/12-PAHSA are consistently reduced in AT depots with HFD while other PAHSA isomers have opposite regulation among the depots (PG WAT versus SQ WAT and BAT) (Figure 3A); and (2) Only two of the five isomers in serum are reduced with HFD (Figure 3A). Thus, PAHSAs undergo isomer-specific and tissue-specific regulation under insulin-resistant conditions in WT mice.

PAHSAs Are Present in Food

To determine whether the changes in PAHSA levels in altered metabolic states could result from differences in dietary intake, we measured PAHSA levels in rodent and human foods. In chow and HFD, we found five of the seven isomers that are present in mouse AT, 13/12-, 11-, 10-, 9-, and 8-PAHSA, but not 7- and 5-PAHSA. However, the relative abundance among isomers was strikingly different from AT or serum with 10-PAHSA being most abundant in both diets (Figure 3B). Levels of all these isomers were substantially lower in HFD than chow (Figure 3B). Given that PAHSAs increase in WAT during fasting (Figures 2D and 2E), regulation of tissue PAHSA levels does not simply reflect dietary intake. Similarly, the abundance of PAHSA isomers in serum and tissues (Figure 2C) does not correlate with predominant isomers

(B) Structural analysis of the 537 ion from AG4OX WAT by tandem MS demonstrates that it is composed of palmitic acid (m/z 255) and hydroxy stearic acid (m/z 299). Octadecanoic acid (m/z 281) results from the dehydration of hydroxy stearic acid. Fragmentation at high collision energies produces two ions at m/z 127 and 155, identifying carbon 9 as the position of the hydroxyl group on hydroxy-stearic acid, confirming the structure to be 9-PAHSA.

(C) Acyl chain carbon numbering scheme, molecular formula, mass and names of FAHFAs from the m/z 537 (PAHSA), m/z 509 (PAHPA), m/z 563 (OAHSA), and m/z 535 (POHSA or OAHPA) ions.

(D) Constituent fatty acid and hydroxy-fatty acid components of FAHFAs. Quantification of 16 FAHFA family members identified in serum of WT and AG4OX mice.

(E) Total PAHSA levels in serum and tissues of WT and AG4OX mice. Inset, liver total PAHSA levels. n = 3–5/group, *$p < 0.05$ versus WT (t test), $^{\dagger}p < 0.05$ versus all other tissues within the same genotype (ANOVA).

(F) Total PAHSA levels in SQ-WAT, PG-WAT, and serum of WT, AG4OX, ChREBP KO, and AG4OX/ChREBP KO mice. n = 3–5/group, *$p < 0.05$ versus all other genotypes within same tissue or serum (ANOVA), # $p < 0.05$ versus AG4OX and ChREBP-KO.

Data are means ± SEM. MRM transitions for detection of different FAHFAs can be found in Table S1.

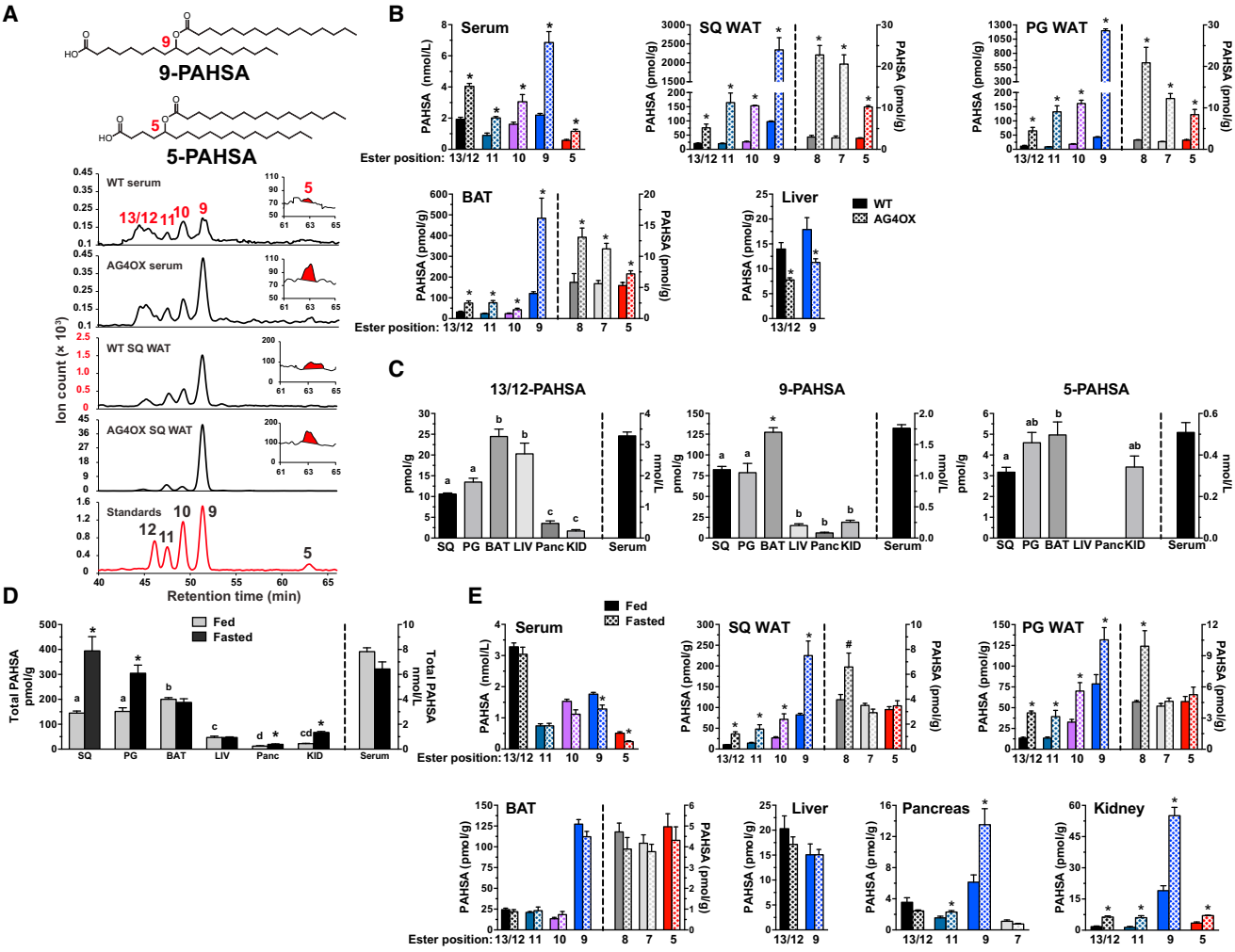

Figure 2. Identification and Quantification of PAHSA Isomers in Mouse Serum and Tissues

(A) Coelution of PAHSA isomers from serum and SQ WAT of WT and AG4OX mice with synthetic standards for individual PAHSA isomers. The peak for 5-PAHSA is shown in red in the inset. Note: different y axis scale for WT SQ WAT (Red numbers) versus AG4OX SQ WAT.

(B) Distribution and quantification of PAHSA isomers in serum and tissues of WT and AG4OX mice. "Ester position" refers to the location of the ester bond in PAHSA isomers. n = 3–5/group, *p < 0.05 versus WT (t test).

(C) Distribution and quantification of 13/12-, 9-, and 5-PAHSA isomers in serum and tissues of WT female FVB mice. n = 3–5/group, [a,b,c] Tissues with different letters are different from each other within the same isomer panel (p < 0.05, ANOVA).

(D and E) Total PAHSA levels (D) and PAHSA isomer levels (E) in serum and tissues of WT mice in fed or fasted (16 hr) states. "Ester position" refers to the location of the ester bond in PAHSA isomers. n = 3–5/group, *p < 0.05, [#] < 0.07 versus fed (t test) [a,b,c,d]Tissues with different letters are different from each other for the fed state (p < 0.05, ANOVA).

Data are means ± SEM. See also Figure S1.

in chow (Figure 3B), suggesting that PAHSAs present in tissues are synthesized endogenously. The fact that 5-PAHSA is not present in mouse chow or HFD (Figure 3B) but is present in WAT, BAT, kidney, and serum (Figures 2A–2C, 2E and 3A) further supports this notion. We also found PAHSAs in all human foods tested with different isomer distributions and abundance (Figure S2C).

PAHSAs Are Synthesized in Mammalian Tissues

To determine whether PAHSAs are synthesized endogenously, we investigated PAHSA biosynthesis in liver and WAT lysates of normal mice. We detected PAHSA biosynthetic activity in both tissues, and it was markedly reduced by heat denaturation (Figure 3C). We also detected PAHSA biosynthesis in vivo. Gavage of mice with 9-hydroxy heptadecanoic acid (9-HHA), a hydroxy fatty acid not normally found in mammalian tissues resulted in synthesis of full-length FAHFAs containing a 9-HHA acyl chain indicating that FAHFAs can be synthesized in vivo (Figure 3D).

PAHSAs Are Present in Humans and Levels Are Reduced with Insulin Resistance

To determine if PAHSAs are present in humans and are regulated in disease states, we measured PAHSA isomers in serum and SQ

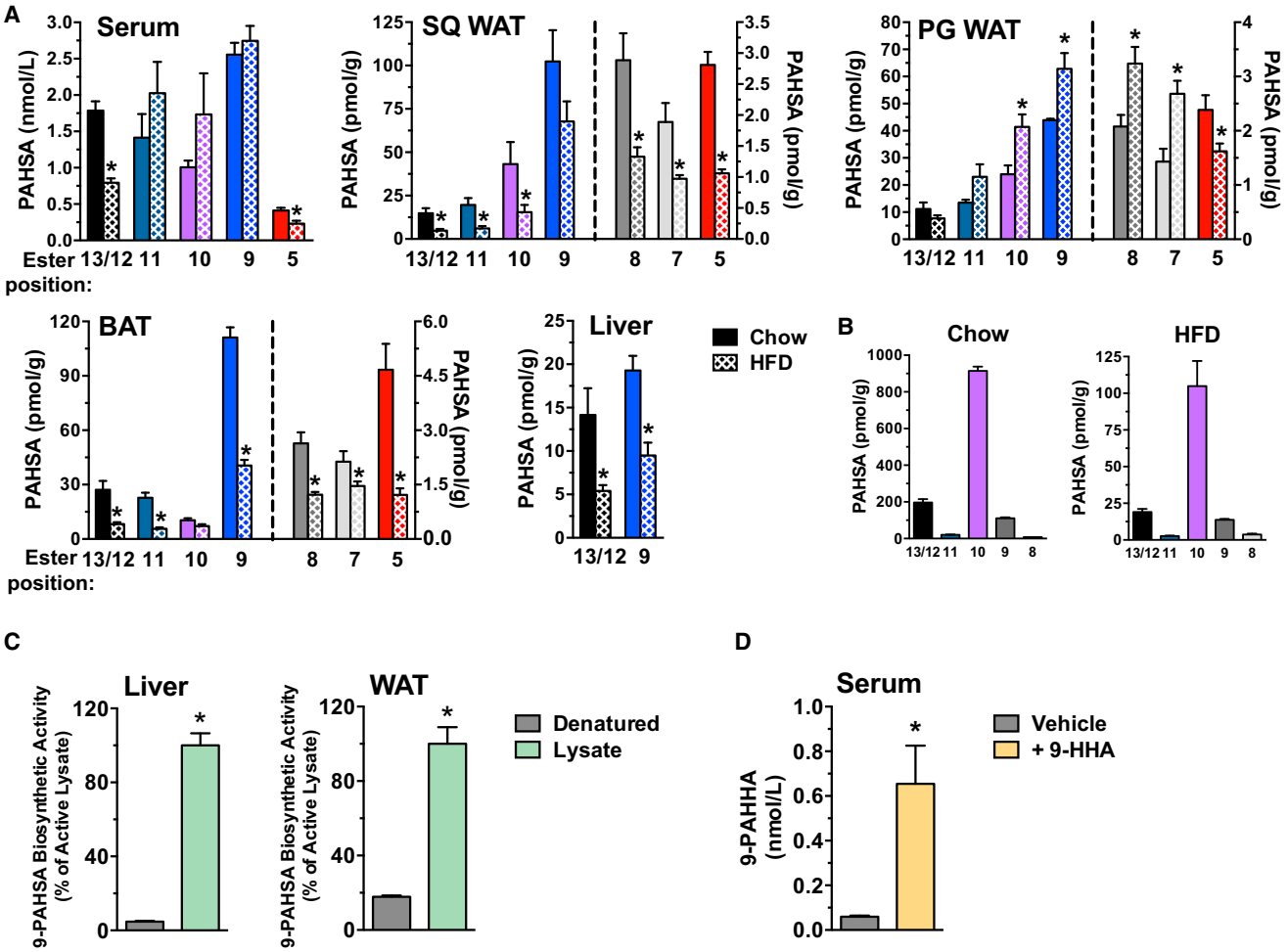

Figure 3. PAHSA Isomer Levels in Tissues of Mice on Chow or HFD, PAHSA Isomer Levels in Food, and PAHSA Biosynthesis In Vivo and in Tissues In Vitro

(A) Quantification of PAHSA isomers in serum, SQ WAT, PG WAT, BAT, and liver of WT female FVB mice fed on chow or HFD for 9 weeks. "Ester position" refers to the location of the ester bond in PAHSA isomers. n = 3–6/group, *p < 0.05 versus chow (t test).

(B) Quantification of PAHSA isomers in mouse chow and HFD. n = 3/group.

(C) 9-PAHSA levels in liver and PG-WAT lysates incubated with palmitoyl-CoA and 9-hydroxy stearic acid and heat-denatured Controls. n = 3/group, *p < 0.05 versus heat-denatured Controls (t test).

(D) 9-palmitic-acid-hydroxy-heptadecanoic-acid (9-PAHHA) serum levels in mice 3 hr postgavage with 9-hydroxy-heptadecanoic-acid (9-HHA) or vehicle control. n = 3/group, *p < 0.05 versus vehicle (t test).

Data are means ± SEM. See also Figure S2.

WAT from insulin-sensitive and insulin-resistant nondiabetic humans. Subjects were middle-aged. BMI was increased in five out of six insulin-resistant participants (Table S2). Insulin resistance was demonstrated by a 61% reduction in glucose infusion rate during a euglycemic hyperinsulinemic clamp (Table S2). Serum triglycerides and free fatty acids in the fasting state were not different between groups (Table S2). Total PAHSA levels are reduced ~40% in serum of insulin-resistant humans (Figure 4A). In serum of both insulin-sensitive and insulin-resistant humans, 9- and 10-PAHSA are most abundant and 13/12- and 5-PAHSAs are present at ~1/5 of these concentrations (Figure 4A). In insulin-resistant people, serum levels of all PAHSAs except 9-PAHSA are reduced by 40%–55% compared to insulin-sensitive people (Figure 4A). Serum concentrations of total PAHSAs and all isomers correlated remarkably strongly with insulin sensitivity measured by clamp (Figure 4B). Serum PAHSA levels did not correlate with levels of nonesterified fatty acids or triglycerides (data not shown) suggesting that PAHSA levels are regulated by different mechanisms.

In human SQ WAT, total PAHSAs are reduced ~70% (Figure 4C). We detected 13/12-, 11-, 10-, 9-, and 5-PAHSA isomers in these biopsies (Figure 4C). However, for technical reasons we were unable to quantify the levels of 11-PAHSA. 9-PAHSA levels were higher than all other isomers (Figure 4C) similar to mouse SQ WAT (Figures 2B, 2E and 3A). 13/12-, 10-, 9-, and 5-PAHSA concentrations in SQ WAT of insulin-resistant people were 60%–73% lower than in insulin-sensitive people (Figure 4C). Concentrations of total PAHSAs and of 9- and 5-PAHSA isomers

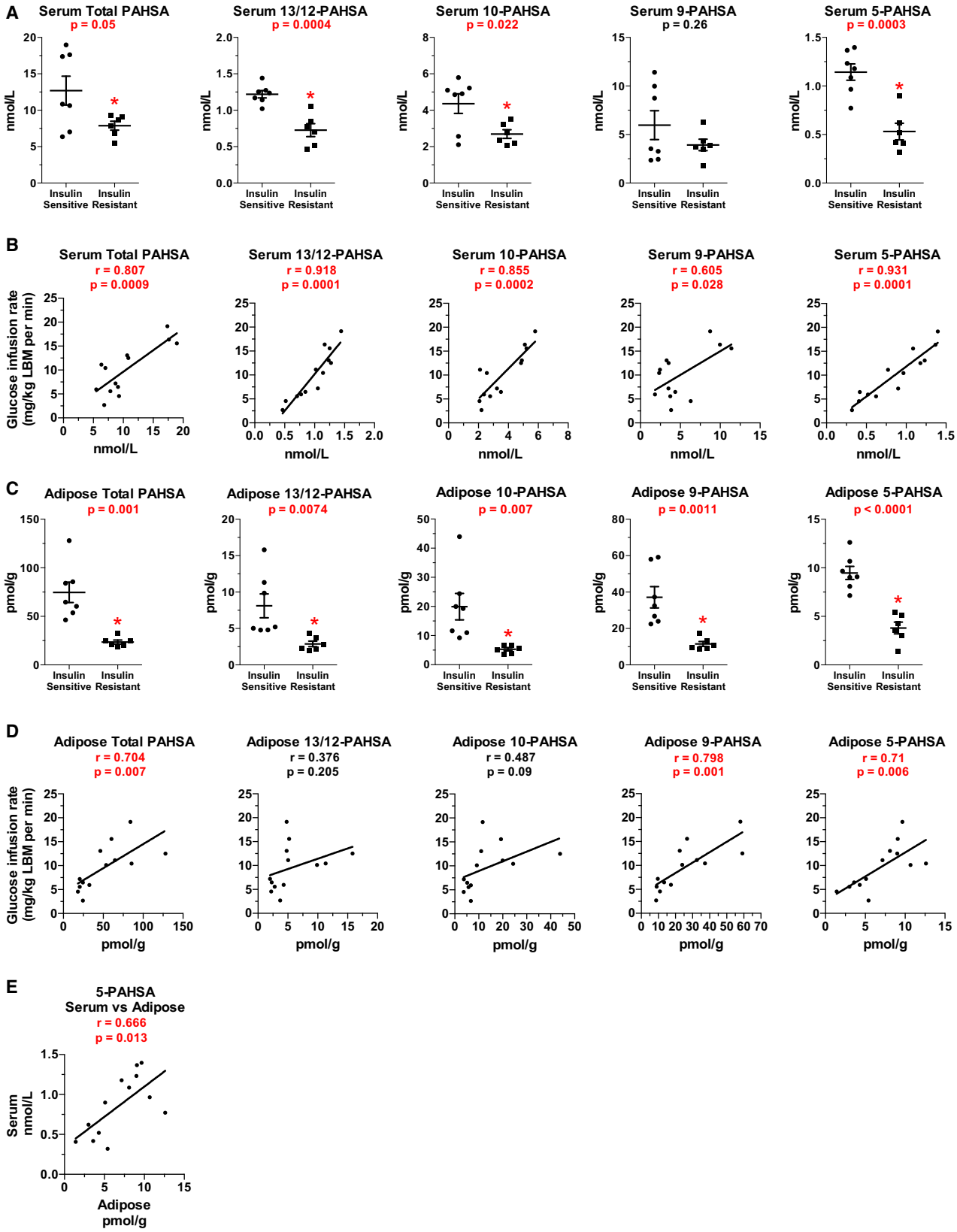

(legend on next page)

in WAT correlate highly with insulin sensitivity (Figure 4D). Serum PAHSA levels correlated with WAT PAHSA levels only for 5-PAHSA (Figure 4E).

In summary, all PAHSA isomers detected are reduced in SQ WAT in insulin-resistant subjects and all but one are reduced in serum. Furthermore, PAHSA levels in serum and WAT correlate highly with whole-body insulin sensitivity. These effects parallel the effects in diet-induced obese mice in which all PAHSA isomers are reduced in SQ WAT, and 13/12- and 5-PAHSA are lower in serum compared to chow-fed mice (Figure 3A). Thus, the regulation of PAHSAs and their inverse correlation with insulin resistance is conserved between mice and humans.

PAHSAs Acutely Improve Glucose Tolerance and Ambient Glycemia

Since levels of PAHSA isomers correlate with insulin sensitivity (Figures 4B and 4D), we tested whether administration of PAHSAs could improve glucose homeostasis in obese, diabetic mice. We selected 9-PAHSA and 5-PAHSA because: (1) 9-PAHSA was the most abundant form in WAT and BAT in WT mice (Figure 2B) and in SQ WAT of humans (Figure 4C). (2) 9-PAHSA is the most strongly upregulated in serum and WAT of insulin-sensitive AG4OX mice (Figure 2B) and was downregulated (with other isomers) in WAT of insulin-resistant humans (Figure 4C). (3) 5-PAHSA was the most consistently downregulated in all adipose depots and in serum of insulin-resistant mice (Figure 3A) and in WAT and serum of insulin-resistant humans. Oral gavage of 5-PAHSA increased serum levels 3- to 5-fold in mice on chow and HFD (Figure S3). As shown in Figure 3A, baseline 5-PAHSA levels were 50%–80% lower in HFD-fed mice compared to chow-fed mice and 5-PAHSA gavage more than restored the levels (Figure S3). The elevation of serum 5-PAHSA levels after gavage in both chow and HFD-fed mice was similar to the elevation in serum of AG4OX mice (Figures 2B and S2). This indicated that PAHSAs are absorbed orally and this route of administration can be used to increase PAHSA concentrations for in vivo metabolic studies.

Acute oral administration of 5- or 9-PAHSA in insulin-resistant HFD-fed mice lowered basal glycemia at 30 min after PAHSA administration (Figure 5A, −30 to 0 min). Subsequently, glucose was administered and we observed improved glucose tolerance in PAHSA-treated mice with reduced area under the glucose excursion curve (Figure 5A). Because of the significant effect of PAHSAs on the baseline glucose levels in HFD-fed mice at 30 min after administration, we tested whether PAHSA action to lower baseline glycemia was sustained. 5-PAHSA or 9-PAHSA had a greater glucose-lowering effect than vehicle treatment in HFD-fed mice also at 2.5–3 hr after administration (Figure 5B). There was no difference in plasma insulin levels at this time in PAHSA-treated compared to vehicle-treated mice (data not shown). Since no food was available during this study, calorie absorption was not a variable and the results suggest that oral PAHSA administration enhances insulin sensitivity. An insulin tolerance test showed lower glucose levels in PAHSA-treated mice compared to vehicle-treated mice for the study duration (120 min after insulin administration) which was largely because of the PAHSA effect to lower baseline glycemia (data not shown).

PAHSAs Stimulate Insulin and GLP-1 Secretion

To determine whether enhanced insulin secretion might contribute to the PAHSA-induced improvement in glucose tolerance (Figure 5A), we tested PAHSA effects on glucose-stimulated insulin secretion (GSIS) in vivo in aged chow-fed mice. 5-PAHSA improved glucose tolerance (Figure 5C) concurrent with acute enhancement of insulin secretion at 5 min after glucose administration (Figure 5D). This may result from direct effects on insulin secretion or from stimulation of incretin secretion since GLP-1 levels were also increased in PAHSA-treated mice at 5 min after glucose administration (Figure 5E). Thus, PAHSAs augment the acute stimulation of GLP-1 and insulin secretion in response to glucose and these effects most likely have an important role in the enhanced glucose tolerance following a single PAHSA dose.

To determine whether the stimulation of insulin secretion is a direct effect of PAHSAs on pancreatic beta cells, we incubated islets from human donors (Table S3, donors' metabolic parameters) with 5-PAHSA and measured GSIS. 5-PAHSA had no effect on insulin secretion at 2.5 mM glucose but augmented the insulin secretion response at 20 mM glucose (Figure 5F). These data demonstrate that 5-PAHSA directly enhances GSIS in human islets. To determine whether PAHSAs directly stimulate GLP-1 secretion, we used the enteroendocrine cell line STC-1. Both 5- and 9-PAHSA rapidly stimulated GLP-1 secretion from STC-1 cells in a dose-dependent manner (Figure 5G). The effects are similar to those with the omega-3 fatty acid, α-linolenic acid, and a synthetic GPR120 ligand (Figure 5G). Thus, the rapid effects of PAHSAs to augment GSIS may be both direct effects on pancreatic beta cells and indirect effects through stimulation of GLP-1 secretion.

PAHSAs Enhance Insulin-Stimulated Glucose Transport and Glut4 Translocation by Activating GPR120

To further understand the mechanism(s) by which PAHSAs improve glucose homeostasis, we tested their effects on glucose transport in adipocytes. PAHSAs increased glucose transport at submaximal and maximal insulin concentrations (Figure 6A). Neither of the fatty acids that form the parent PAHSA structure,

Figure 4. PAHSA Levels Are Decreased in Insulin-Resistant Humans and Levels Correlate with Insulin Sensitivity

(A) Quantification of total PAHSAs and individual PAHSA isomers in serum of insulin-sensitive and insulin-resistant nondiabetic humans (see Table S2 for metabolic characteristics). n = 6–7/group.

(B) Correlation between insulin-sensitivity (clamp glucose infusion rate) and serum total PAHSA and individual PAHSA isomers. n = 13.

(C) Quantification of total PAHSA and individual PAHSA isomers in SQ WAT of insulin-sensitive and insulin-resistant humans. n = 6–7/group.

(D) Correlation between insulin-sensitivity (clamp glucose infusion rate) and SQ WAT total PAHSA and individual PAHSA isomers. n = 13.

(E) Correlation between SQ WAT and serum 5-PAHSA levels. LBM: lean body mass. Individual p values are shown on graphs, *$p < 0.05$ versus insulin-sensitive (t test, A and C).

Data are means ± SEM for (A and C). Correlations were determined by linear regression analysis for (B, D, and E).

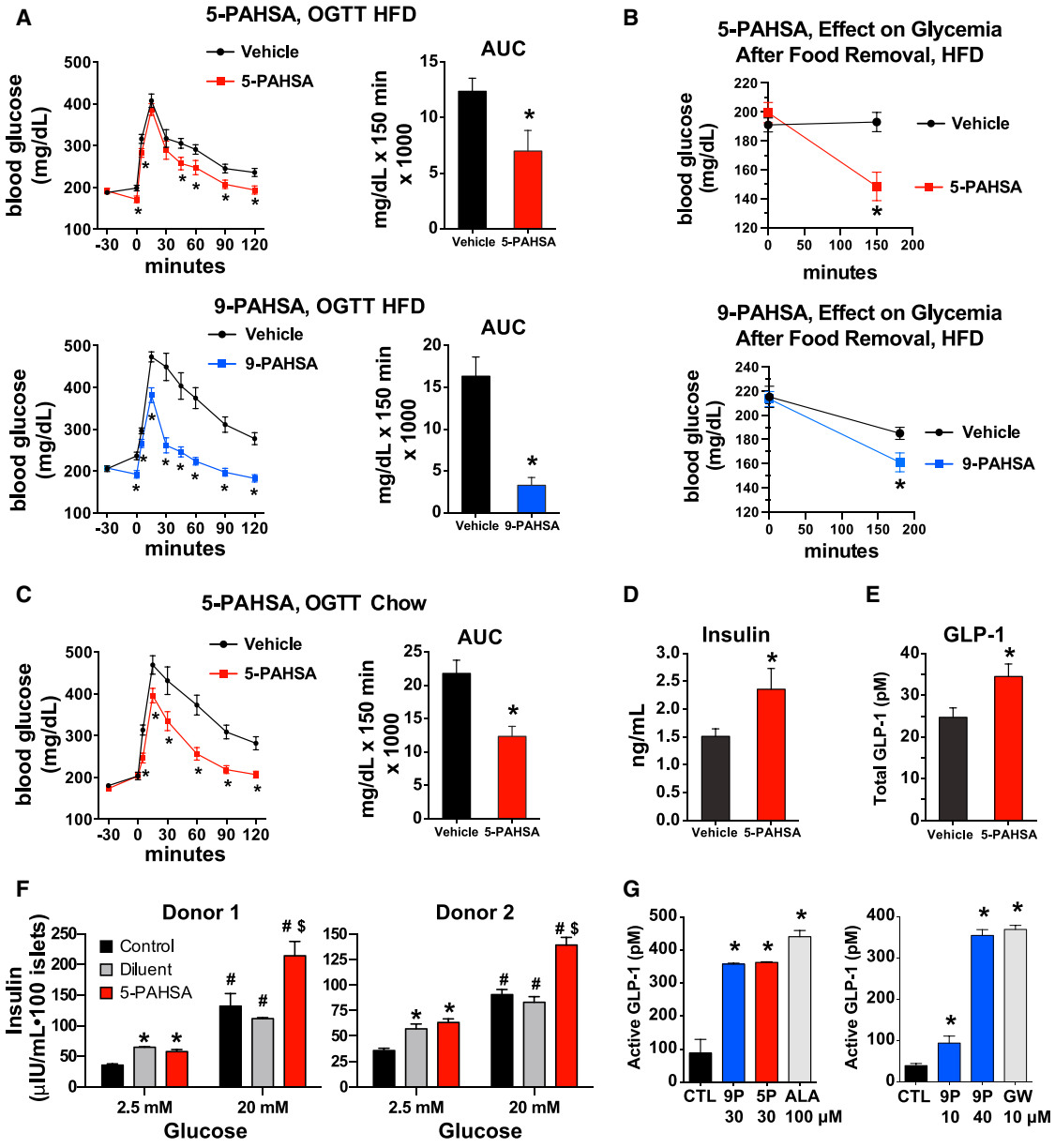

Figure 5. PAHSAs Improve Glucose Tolerance and Ambient Glycemia In Vivo and Augment Insulin and GLP-1 Secretion

(A) 4.5 hr after food removal, HFD-fed mice were gavaged with 5-PAHSA (top), 9-PAHSA (bottom) or vehicle control. 30 min later an oral glucose tolerance test (OGTT) was performed. n = 12–14/group, mice were on HFD for 42–52 weeks. *p < 0.05 versus vehicle at same time (t test). Area under the curve (AUC) was calculated from −30 to 120 min. *p < 0.05 versus vehicle (t test).

(B) 2.5 hr after food removal, HFD-fed mice were gavaged with 5-PAHSA (top), 9-PAHSA (bottom) or vehicle control. Glycemia was measured immediately before (time 0) and at 2.5 hr (5-PAHSA) or 3 hr (9-PAHSA) after PAHSA gavage. n = 12–14/group. *p < 0.05 versus vehicle (t test).

(C) 4.5 hr after food removal, aged, chow-fed mice (45-week-old) were gavaged with 5-PAHSA 30 min prior to an OGTT. n = 12–14/group. *p < 0.05 versus vehicle at same time (t test). Area under the curve (AUC) was calculated from −30 to 120 min. *p < 0.05 versus vehicle (t test).

(D and E) Serum insulin levels (D) and serum GLP-1 levels (E) 5 min postglucose challenge in chow-fed mice gavaged with 5-PAHSA or vehicle (glucose values shown in C). n = 12–14/group, *p < 0.05 versus vehicle (t test).

(F) Insulin secretion from primary human islets from two independent donors. Islets were incubated with low (2.5 mM) or high (20 mM) glucose ex vivo in the presence of 5-PAHSA (20 μM) or Control (KRB buffer). Diluent for 5-PAHSA was methanol (0.25%). n = 100 islets/condition, *p < 0.05 versus control 2.5 mM glucose (t test), #p < 0.05 versus all treatments at 2.5 mM glucose (t test), $p < 0.05 versus control and diluent at 20 mM glucose (t test).

(G) Active GLP-1 secretion from STC-1 cells in response to 5-PAHSA (5P), 9-PAHSA (9P), α-Linolenic Acid (ALA), GW9508 (GW), or vehicle control (CTL, DMSO). n = 4/group, *p < 0.05 versus vehicle (CTL) (t test).

Data are means ± SEM. See also Table S3 and Figure S3.

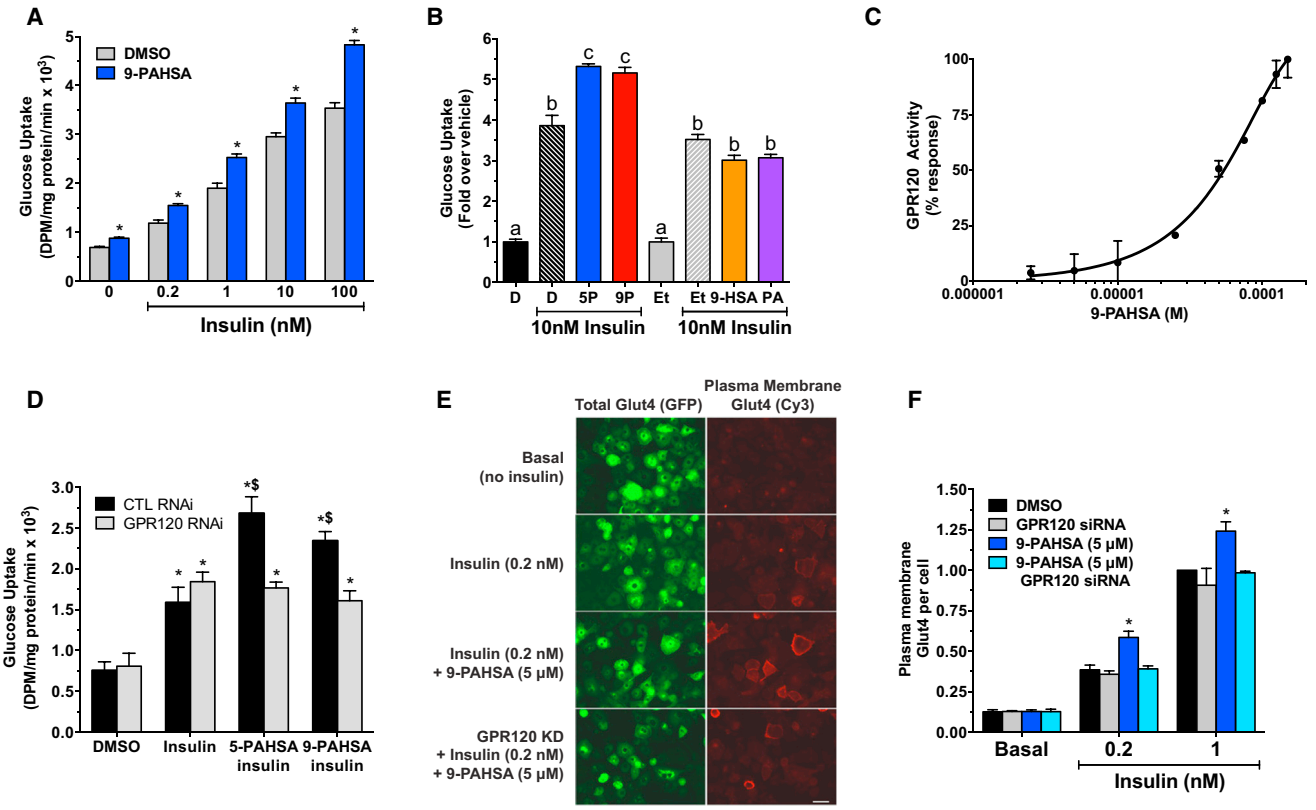

Figure 6. PAHSAs Regulate Glucose Uptake and Glut4 Translocation via GPR120

(A) Insulin-stimulated glucose transport in 3T3-L1 adipocytes treated with 9-PAHSA (20 μM) or vehicle (DMSO) control for 6 days. n = 6/group, *p < 0.001 versus vehicle (DMSO) at the same insulin concentration (ANOVA).

(B) Glucose transport in 3T3-L1 adipocytes treated for 48 hr with 9-PAHSA, 5-PAHSA, palmitic acid (PA), 9-hydroxy stearic acid (HSA) at 20 μM or their respective vehicle controls (DMSO for 9- and 5-PAHSA. Ethanol for PA and HSA). n = 6/group. [a,b,c]groups with different letters are different from each other p < 0.05 (ANOVA).

(C) Dose response of 9-PAHSA on GPR120 binding and receptor activation. n = 3 wells/condition.

(D) Insulin (10 nM)-stimulated glucose transport in 3T3-L1 adipocytes transfected with control siRNA (CTL) or GPR120 siRNA and treated with 5-PAHSA (10 μM), 9-PAHSA (10 μM) or vehicle (DMSO) control for 2 days. n = 3/group, *p < 0.05 versus control siRNA or GPR120 siRNA with DMSO without insulin (ANOVA), [$]p < 0.05 versus all other conditions except each other (ANOVA).

(E) Glut4 plasma membrane translocation in 3T3-L1 adipocytes transfected with control siRNA or GPR120 siRNA and treated with 9-PAHSA in the presence or absence of insulin. Scale bar = 50 μm.

(F) Quantification of Glut4 translocation in (E). Bars show means of six independent experiments without siRNA knockdown and three with siRNA knockdown. Each experiment had an n ≥ 50 cells/condition.*p < 0.05 versus everything else at same insulin concentration (ANOVA). All data are means ± SEM. See also Figure S4.

palmitic acid or hydroxystearic acid, alone improved insulin-stimulated glucose transport (Figure 6B). The effects of PAHSAs on insulin-stimulated glucose transport occurred with both acute (30 min) and chronic (2–6 day) treatment and at concentrations as low as 500 nM (Figure S4A). PAHSAs did not alter total cellular Glut1 or Glut4 protein levels in adipocytes even after 6 days of incubation (data not shown).

Bioactive lipids can influence biology through binding to cell surface receptors such as G protein-coupled receptors (GPCRs) (Hara et al., 2013). The effects of PAHSAs on GLP-1 secretion and glucose transport are consistent with possible activation of GPCRs (Hirasawa et al., 2005). To determine whether PAHSAs activate GPCRs, we screened a panel of known lipid-activated GPCRs. Both 9-PAHSA (Figure 6C) and 5-PAHSA (data not shown) dose-dependently bind to and activate GPR120 which is also activated by ω-3 fatty acids and monounsaturated fatty acids (Hirasawa et al., 2005; Oh et al., 2010). Activation of GPR120 increases glucose transport and Glut4 translocation in adipocytes (Oh et al., 2010). To test whether GPR120 mediates the effects of PAHSAs, we knocked it down >95% in adipocytes with siRNA (Figure S4B). This completely reversed the enhanced effects of PAHSAs on insulin-stimulated glucose transport (Figure 6D). These data demonstrate that GPR120 mediates the effects of PAHSAs on insulin-stimulated glucose transport.

To determine the mechanism for enhancement of glucose transport with PAHSAs, we analyzed the effects on insulin-induced Glut4 translocation to the plasma membrane in adipocytes. In the absence of insulin, PAHSAs had no effect on Glut4 translocation (Figure 6F). However, PAHSAs enhanced Glut4 translocation at submaximal and maximal insulin

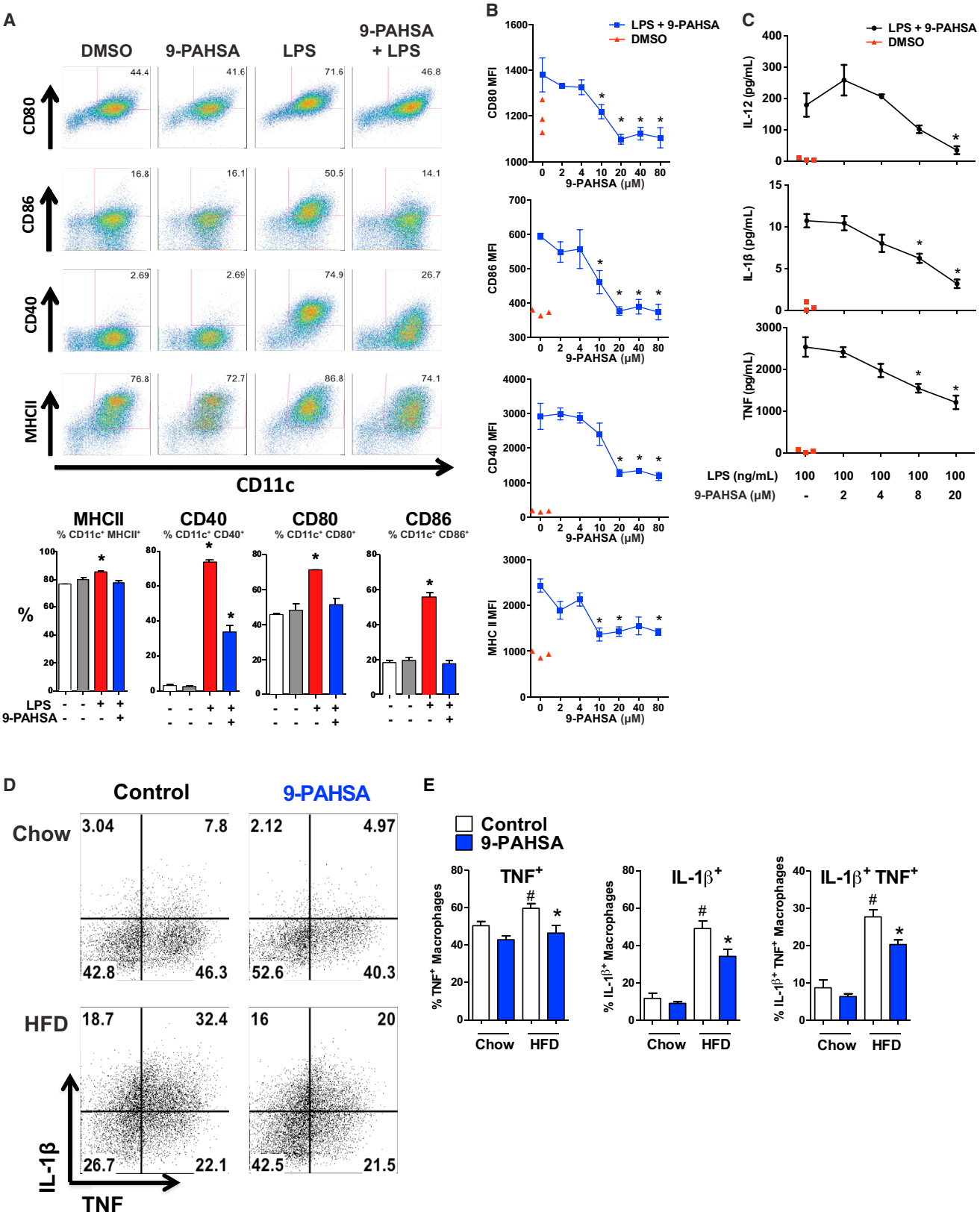

(legend on next page)

concentrations (Figures 6E and 6F). These data indicate that PAHSAs augment insulin-stimulated glucose transport by enhancing Glut4 translocation. Knockdown of GPR120 in adipocytes completely blocked the effect of PAHSAs to augment insulin-stimulated Glut4 translocation (Figures 6E and 6F). We obtained this effect with two different GPR120 siRNAs indicating that it is a specific "on target" effect. These data together demonstrate that PAHSAs bind to and activate GPR120 (Figure 6C), which mediates the effects of PAHSAs on insulin-stimulated glucose transport and Glut4 translocation (Figures 6D–6F).

PAHSAs Exert Anti-Inflammatory Effects

Fatty acids, such as ω-3 fatty acids, can elicit anti-inflammatory effects through GPR120 (Oh et al., 2010). GPR120 is expressed in bone-marrow-derived dendritic cells (BMDCs), which are initial antigen-presenting cells in the innate immune response. Innate immunity is activated in WAT in obesity and may contribute to the insulin-resistant state (Lumeng and Saltiel, 2011). Saturated fatty acids such as palmitic acid and pathogen-derived molecules, such as lipopolysaccharide (LPS), promote BMDC maturation by activating Toll-like receptors (TLRs) (Lumeng and Saltiel, 2011). This induces expression of proinflammatory cytokines, major histocompatibility complex II (MHC II), and costimulatory molecules (CD40, CD80, and CD86) required for antigen presentation and T cell activation. LPS addition to BMDCs robustly increased CD80, CD86, CD40, and MHC II expression, demonstrating the expected activation of BMDCs (Figure 7A). 9-PAHSA blocked the LPS effect on BMDC activation as evidenced by inhibition of LPS-induced CD80, CD86, CD40, and MHC II expression (Figures 7A and 7B). Neither palmitic acid which is a component of the PAHSA molecule, nor the mono-unsaturated fatty acid, oleic acid, exerted these effects at a concentration (20 μM) (Figure S5) at which 9-PAHSA had strong anti-inflammatory effects (Figure 7B). 9-PAHSA completely blocked LPS-induced IL-12 secretion in a dose-dependent manner (Figure 7C) and substantially reduced IL-1β and TNFα at doses as low as 8 μM (Figure 7C). These data indicate that 9-PAHSA has anti-inflammatory effects.

To test whether PAHSAs exert anti-inflammatory effects in vivo, we measured TNFα and IL-1β in AT macrophages (ATMs) from HFD-fed mice gavaged with 9-PAHSA or vehicle for 3 days. The percentage of ATMs expressing TNFα, IL-1β, or both was elevated in HFD-fed mice compared to chow. Administration of 9-PAHSA normalized the percentage of TNFα positive ATMs and reduced the percentage of IL-1β positive and double-positive ATMs (Figure 7D). Total ATM number was not reduced due to the short treatment duration (data not shown). This demonstrates that PAHSAs have anti-inflammatory effects in vivo. Therefore, reduced PAHSA levels in insulin-resistant states (Figures 3A and 4) could contribute to activation of the innate immune system, thus playing a role in AT inflammation and systemic insulin-resistance.

DISCUSSION

Adipose-Glut4 levels in humans are tightly associated with insulin sensitivity and lower Glut4 levels confer increased T2D risk (Carvalho et al., 2001; Shepherd and Kahn, 1999). Adipose-specific Glut4 overexpression in mice (AG4OX) causes beneficial metabolic effects which result from enhanced ChREBP-driven de novo lipogenesis in adipose tissue (AT) (Herman et al., 2012; Tozzo et al., 1995). Because this occurs even in the setting of obesity and elevated serum fatty acids (Herman et al., 2012; Tozzo et al., 1995), we sought to determine whether the augmented lipogenesis in AG4OX mice leads to production of lipid species that have favorable metabolic effects. Here we report the discovery of a class of mammalian lipids characterized by a branched ester linkage between a fatty-acid and a hydroxy-fatty acid or FAHFAs. The closest reported structures are (O-acyl)-omega hydroxy-fatty acids in the eye (Butovich et al., 2009), which are not branched.

Of the 16 FAHFA family members we report here, we extensively characterized the biology of PAHSA isomers that are present in many, if not all, tissues and in serum in normal mice and in human WAT and serum (Figures 1, 2, 3, and 4). Total PAHSA levels are highest in WAT and BAT that also have the greatest number of PAHSA isomers (Figure 2). Furthermore, PAHSA levels are highly elevated in serum, WAT and BAT of AG4OX mice that are obese but have markedly enhanced glucose tolerance (Herman et al., 2012; Shepherd et al., 1993). In parallel, nearly all PAHSA isomers are higher in serum and SQ WAT of insulin-sensitive humans compared to insulin-resistant humans.

In insulin-resistant, obese mice, PAHSA isomer levels show adipose-depot-specific regulation and all PAHSA isomers are lower in SQ WAT of obese compared to lean mice (Figure 3). These results in SQ WAT are similar to those in insulin-resistant

Figure 7. 9-PAHSA Inhibits LPS-Induced Dendritic Cell Maturation In Vitro and Proinflammatory Cytokine Production from Adipose Tissue Macrophages In Vivo

(A) LPS induces dendritic cell (DC) maturation (increased percentage of $CD11c^+$ cells expressing costimulatory molecules, CD80, CD86, CD40, and MHCII). This LPS effect is reduced in the presence of 9-PAHSA (40 μM) compared to vehicle (DMSO) control. Quantification of $CD11c^+$ cells which are positive for costimulatory molecules from the panel above. n = 3 mice/group.

(B) LPS-induced DC maturation is inhibited by increasing concentrations of 9-PAHSA. Red triangles represent vehicle for 9-PAHSA (DMSO) without LPS. MFI: median fluorescence intensity. n = 3 mice/group.

(C) LPS–induced cytokine secretion from DC's is inhibited by increasing concentrations of 9-PAHSA compared to vehicle for 9-PAHSA (DMSO, "-") control. Red triangles represent vehicle for 9-PAHSA (DMSO, "-") without LPS. n = 3 mice/group.

(D) Flow cytometry representation of AT macrophages expressing TNFα and IL-1β. Mice fed on HFD or chow mice were gavaged for 3 days with 9-PAHSA (30 mg/kg for chow mice and 45 mg/kg for HFD mice) or vehicle control. PG-WAT was harvested on day 4 and the stromal vascular cells were incubated in vitro with PMA, ionomycin and brefeldin for 5 hr. AT macrophages ($CD45^+CD11b^+F4/80^+$) were stained intracellularly for TNFα and IL-1β.

(E) Quantification D-percentage of AT macrophages expressing TNFα, IL-1β or both. n = 5 mice/group. LPS concentration is 100 ng/ml for all panels.

*$p < 0.05$ versus LPS-activated cells without PAHSA treatment (A–C) or control cells, same diet (E) by one-way (A–C) and two-way ANOVA (D). #$p < 0.05$ versus all other groups by two-way ANOVA. Data are means ± SEM. See also Figure S5.

people (Figure 4). 5-PAHSA is consistently reduced in all adipose depots studied and in serum in insulin-resistant mice and humans. In insulin-resistant people, most PAHSA isomers are reduced in serum and AT and correlate highly with insulin sensitivity (Figure 4). ChREBP is required to maintain normal PAHSA levels in WT mice and elevated levels in AG4OX mice (Figure 1F). In humans, ChREBP and lipogenic enzyme expression correlate strongly with insulin-sensitivity. Thus, the reduction in PAHSAs in insulin-resistant people may be mediated by suppressed ChREBP expression.

This class of lipids has multiple effects that improve glucose-insulin homeostasis which suggests that restoring PAHSA levels in insulin-resistant people could have beneficial metabolic effects. Oral PAHSA administration in insulin-resistant mice on a HFD rapidly lowers ambient glucose and also improves glucose tolerance (Figures 5A and 5B). This may result, at least in part, from enhanced glucose transport since PAHSAs augment insulin-stimulated glucose transport and Glut4 translocation directly in adipocytes in vitro (Figure 6). In addition, PAHSAs stimulate both insulin and GLP-1 secretion (Figures 5D–5G). Importantly, the effects of PAHSAs on insulin secretion are observed only under hyperglycemic conditions (Figure 5F). The enhanced GSIS in vivo most likely results from both direct effects on islet cells and indirect effects though GLP-1-stimulated insulin secretion.

Total PAHSA levels in tissues and serum are similar to concentrations of signaling lipids such as prostacyclins, prostaglandins, steroids, and endocannabinoids. PAHSAs are signaling lipids that directly bind to and activate GPR120 in a cell-based GPCR activity assay (Figure 6C). GPR120 activation appears to explain the effects on insulin-induced Glut4 translocation and glucose uptake in adipocytes (Figures 6B–6D) and may explain the effects on GLP-1 secretion and inhibition of inflammatory responses in immune cells. Thus, PAHSAs are endogenous GPR120 ligands and may also exert effects through other lipid-activated GPCRs.

PAHSAs have striking anti-inflammatory effects and largely block LPS-stimulated dendritic cell activation and cytokine production (Figure 7). Chronic, low-grade inflammation in AT plays an important role in obesity-related insulin resistance (Lumeng and Saltiel, 2011; Olefsky and Glass, 2010). Three days of PAHSA gavage in HFD-fed mice reduced the percentage of ATMs that express proinflammatory cytokines (Figure 7D). Therefore, anti-inflammatory effects of PAHSAs may promote insulin sensitivity and ameliorate other inflammatory diseases.

Insulin-sensitizing and anti-inflammatory effects and GLP-1 secretion are also observed with ω-3 fatty acids (Hirasawa et al., 2005; Oh et al., 2010). However, a major difference between ω-3 fatty acids and PAHSAs is that PAHSAs are synthesized endogenously as evidenced by PAHSA biosynthetic activity in adipose and liver lysates and incorporation of modified precursors into FAHFAs in vivo (Figures 3C and 3D). The potential importance of identifying an endogenous GPR120 ligand is demonstrated by the fact that loss of function mutations in GPR120 in humans promote obesity and insulin resistance (Ichimura et al., 2012). Thus, GPR120 is an important control point in the integration of anti-inflammatory and systemic insulin-sensitizing responses and is emerging as an important regulator of whole-body glucose-insulin homeostasis (Mo et al., 2013). It is the subject of ongoing preclinical investigation for the treatment of obesity-related insulin resistance, T2D, and inflammatory diseases (Mo et al., 2013; Oh et al., 2014).

Reduced PAHSA levels may contribute to diabetes risk since many PAHSA isomers are reduced in SQ WAT and serum of insulin-resistant rodents (Figure 3A) and humans (Figure 4). In humans, PAHSA levels in both serum and SQ WAT correlate highly with whole-body insulin-sensitivity (Figures 4B and 4D). Thus, reduced circulating PAHSA levels may serve as a biomarker for insulin resistance and T2D risk. PAHSAs lower glycemia, improve glucose tolerance and stimulate GLP-1 and insulin secretion in mice (Figure 5). This raises the possibility that restoring the reduced PAHSA levels in insulin-resistant humans could have therapeutic effects to prevent or ameliorate insulin resistance and T2D. The discovery of the FAHFAs is important also because their presence suggests uncharacterized biochemical pathways and enzymes that may be important in human physiology and disease. Changes in the levels of these metabolites and in their signaling pathways may provide important insights and new treatment avenues for metabolic and inflammatory diseases.

EXPERIMENTAL PROCEDURES

Materials and Reagents

All chemicals were purchased from Sigma-Aldrich (St. Louis, MO) unless otherwise stated.

Culture and Differentiation of Cells

3T3-L1 fibroblasts were cultured and differentiated as described (Norseen et al., 2012). STC-1 cells were maintained in DMEM supplemented with 10% FCS, pen/strep and maintained at 37°C and 5% CO_2.

Pancreatic Islets, GSIS, and GLP-1 Secretion Studies

Human islets from nondiabetic donors were obtained from Prodo Laboratories (Irvine, CA). GSIS studies (Kowluru et al., 2010) and GLP-1 secretion from STC-1 cells (Hirasawa et al., 2005) were performed as described.

Generation and Treatment of Bone-Marrow-Derived Dendritic Cells

BMDCs were generated as described (Moraes-Vieira et al., 2014). Cells were incubated with 9-PAHSA 10 min prior to LPS (100 ng/ml) stimulation. CD11c, MHC II, CD40, CD80 and CD86 (all Biolegend) were detected by flow cytometry as described (Moraes-Vieira et al., 2014). Cytokine levels were measured by ELISA (Biolegend).

9-PAHSA Biosynthetic Activity Assay

Liver and PG-WAT tissue was Dounce homogenized in buffer A (10 mM Tris-HCL (pH 7.4), 250 mM Sucrose containing protease inhibiters (Roche)). Lysates were centrifuged at 1,200 g to remove incompletely lysed cells and debris. Lysates were then adjusted to 1 mg/ml protein and 100 μl was incubated with 100 μM palmitoyl-CoA and 100 μM 9-hydroxy stearic acid (PAHSA substrates) for 2 hr at 37°C. Control samples were heat denatured by boiling for 10 min prior to incubation with PAHSA substrates. After 2 hr the reaction was stopped by the addition of 300 μl cold buffer A followed by 400 μl of methanol (MeOH) and 800 μl of chloroform. Samples were vortexed and centrifuged at 1,200 g for 5 min. 9-PAHSA levels in the organic layer were measured by LC-MS.

FAHFA Synthesis In Vivo

Two hours postfood removal C57B6/J mice were gavaged with 25 mg/Kg of 9-hydroxy heptadecanoic acid or vehicle. Three hours later mice were sacrificed and serum was collected. Serum lipids were extracted and 9-PAHHA levels measured by LC-MS.

Animal Studies and Measurement of Metabolic Parameters

Female AG4OX mice and WT FVB littermate controls (Shepherd et al., 1993) at 8–14 weeks old were used for FAHFA tissue distribution and regulation with fasting and HFD studies. ChREBP-KO, ChREBP-KO/AG4OX and control females (Herman et al., 2012) were used at 16–18 weeks old. Mice were fed on chow (Lab Diet, 5008) or HFD (Harlan Teklad, TD.93075) for 9 weeks (female FVB) or 42–52 weeks (male C57BL6/J). OGTT's were performed as described (Moraes-Vieira et al., 2014) after 5 hr food removal.

Anti-Inflammatory Effects of 9-PAHSA In Vivo

Male C57BL6/J mice on chow or HFD described above were gavaged once a day for 3 days with 30 mg/kg (chow) or 45 mg/kg (HFD) of 9-PAHSA or an equivalent volume of vehicle. On the 4th day PG stromal vascular fraction (SVF) cells were harvested and cultured for 5 hr with ionomycin, PMA and brefeldin at 37°C and the intracellular cytokine content was measured in gated CD45$^+$, CD11b$^+$, and F4/80$^+$ cells as described (Moraes-Vieira et al., 2014).

Human Studies

Hyperinsulinemic-euglycemic clamp was performed in 13 nondiabetic subjects. SQ WAT biopsies were obtained from the peri-umbilical, abdominal region after an overnight fast.

Lipid Extraction

Lipid extraction was performed as described (Bligh and Dyer, 1959; Saghatelian et al., 2004). Tissues (60–150 mg) were Dounce homogenized on ice in a mixture of 1.5 ml MeOH, 1.5 ml chloroform and 3 ml citric acid buffer. PAHSA standards were added to chloroform prior to extraction. The resulting mixture was centrifuged and the organic phase containing extracted lipids was dried under N_2 and stored at −80°C prior to solid phase extraction.

Lipidomic Analysis

Lipidomic analysis was performed using an Agilent 6220 ESI-TOF fitted with an electrospray ionization source with a capillary voltage of 3,500 kV and fragmentor voltage of 100 V. A Gemini C18 reversed phase column (Phenomenex) and a C18 reversed phase guard column (Western Analytical) was used for LC-MS analysis in negative mode. In positive mode, a Luna C5 reversed phase column (Phenomenex) was used together with a C4 reversed phase guard column (Western Analytical). Drying gas temperature was 350°C, flow rate 10 l/min and nebulizer pressure 45 psi. Untargeted data were collected using an m/z of 100–1,500.

ADD

Structural characterization of the FAHFAs by MS/MS was carried out on an Agilent 6510 quadrupole-time of flight MS.

Synthesis of PAHSAs and PAHSA Standards

Detailed information on synthesis of PAHSAs and PAHSA standards is outlined in the Supplemental Information.

Targeted LC/MS Analysis of FAHFAs

FAHFAs were measured on an Agilent 6410 Triple Quad LC/MS via Multiple Reaction Monitoring in negative ionization mode. Extracted and fractionated samples were reconstituted in 25 μl MeOH; 10 μl was injected for analysis. A Luna C18(2) (Phenomenex) column was used with an in-line filter (Phenomenex). Distinct PAHSA species were resolved via isocratic flow at 0.2 ml/min for 120 min using 93:7 MeOH:H_2O with 5 mM ammonium acetate and 0.01% ammonium hydroxide as solvent. Transitions for endogenous PAHSAs were m/z 537.5 → m/z 255.2 (Collision Energy [CE] = 30 V), m/z 537.5 → m/z 281.2 (CE = 25 V), and m/z 537.5 → m/z 299.3 (CE = 23 V), and the transition for ^{13}C-9-PAHSA was m/z 553.5 → m/z 271.3 (CE = 30 V), all FAHFA transitions are listed in Supplemental Information.

Data Analysis

All values are means ± SEM. Differences between groups were assessed using unpaired two-tailed Student's t tests and/or ANOVA with Fisher's LSD multiple comparisons as specified in figure legends. All statistical analyses were performed with GraphPad Prism 5.

SUPPLEMENTAL INFORMATION

Supplemental Information includes Extended Experimental Procedures, four figures, four tables, and one data file and can be found with this article online at http://dx.doi.org/10.1016/j.cell.2014.09.035.

AUTHOR CONTRIBUTIONS

M.M.Y. and I.S. conceived of, designed, performed, and interpreted experiments and made figures. P.M.M.-V. designed, performed and interpreted the immunology experiments and made the figures. M.A.H. conceived of the untargeted lipidomics experiment and E.A.H. and M.A.H. designed and performed the untargeted lipidomics experiment. E.A.H. designed, performed and interpreted the data from the structure elucidation studies. E.A.H. and A.S. designed and performed chemical synthesis of the lipids. T.Z., I.S., E.A.H. and S.C. developed and applied new targeted lipidomics methods. J.L., A.S.D., O.D.P. assisted with animal studies. B.B.K., I.S., U.S., and A.H. designed, performed and interpreted the data from human studies. R.T.P, T.E.M. designed and performed Glut4 translocation assays. B.B.K. and A.S. conceived of, designed and supervised the experimental plan and interpreted experiments. B.B.K., A.S., M.M.Y. and I.S. wrote the manuscript. M.A.H., P.M.M.V., O.D.P., T.E.M., and J.L. edited the manuscript.

ACKNOWLEDGMENTS

We thank Dr. Thue Schwartz for stimulating discussions; Drs. Anna Greka and Dequan Tian for performing functional assays; Pratik Aryal, Marlee Jackson, Kerry Wellenstein, and Peter Dwyer for technical assistance; and Dr. Douglas Hanahan for the STC1 cells. Supported by grants from the NIH R37DK43051 and P30 DK57521 (B.B.K.); R01 DK098002 (B.B.K. and T.E.M.); a grant from the JPB foundation (B.B.K.). Searle Scholars Award, Burroughs Welcome Fund CABS, and Sloan Foundation Fellowship (A.S.); Harvard Training Program in Nutrition and Metabolism, 2T32HD052961 (M.M.Y.); 5T32DK007516 (B.B.K., M.M.Y., and J.L.); K08 DK076726 (M.A.H.); P30 DK046200 (M.A.H.). B.B.K., M.A.H., A.S., and E.A.H. are inventors on a patent related to the fatty acid hydroxy-fatty acids.

Received: March 23, 2014
Revised: July 15, 2014
Accepted: September 18, 2014
Published: October 9, 2014

REFERENCES

Abel, E.D., Peroni, O., Kim, J.K., Kim, Y.B., Boss, O., Hadro, E., Minnemann, T., Shulman, G.I., and Kahn, B.B. (2001). Adipose-selective targeting of the GLUT4 gene impairs insulin action in muscle and liver. Nature *409*, 729–733.

Benhamed, F., Denechaud, P.D., Lemoine, M., Robichon, C., Moldes, M., Bertrand-Michel, J., Ratziu, V., Serfaty, L., Housset, C., Capeau, J., et al. (2012). The lipogenic transcription factor ChREBP dissociates hepatic steatosis from insulin resistance in mice and humans. J. Clin. Invest. *122*, 2176–2194.

Bligh, E.G., and Dyer, W.J. (1959). A rapid method of total lipid extraction and purification. Can. J. Biochem. Physiol. *37*, 911–917.

Boden, G., and Shulman, G.I. (2002). Free fatty acids in obesity and type 2 diabetes: defining their role in the development of insulin resistance and beta-cell dysfunction. Eur. J. Clin. Invest. *32* (*Suppl 3*), 14–23.

Bruss, M.D., Khambatta, C.F., Ruby, M.A., Aggarwal, I., and Hellerstein, M.K. (2010). Calorie restriction increases fatty acid synthesis and whole body fat oxidation rates. Am. J. Physiol. Endocrinol. Metab. *298*, E108–E116.

Butovich, I.A., Wojtowicz, J.C., and Molai, M. (2009). Human tear film and meibum. Very long chain wax esters and (O-acyl)-omega-hydroxy fatty acids of meibum. J. Lipid Res. *50*, 2471–2485.

Cao, H., Gerhold, K., Mayers, J.R., Wiest, M.M., Watkins, S.M., and Hotamisligil, G.S. (2008). Identification of a lipokine, a lipid hormone linking adipose tissue to systemic metabolism. Cell *134*, 933–944.

Carvalho, E., Jansson, P.A., Nagaev, I., Wenthzel, A.M., and Smith, U. (2001). Insulin resistance with low cellular IRS-1 expression is also associated with low GLUT4 expression and impaired insulin-stimulated glucose transport. FASEB J. *15*, 1101–1103.

Carvalho, E., Kotani, K., Peroni, O.D., and Kahn, B.B. (2005). Adipose-specific overexpression of GLUT4 reverses insulin resistance and diabetes in mice lacking GLUT4 selectively in muscle. Am. J. Physiol. Endocrinol. Metab. *289*, E551–E561.

Hara, T., Kimura, I., Inoue, D., Ichimura, A., and Hirasawa, A. (2013). Free fatty acid receptors and their role in regulation of energy metabolism. Rev. Physiol. Biochem. Pharmacol. *164*, 77–116.

Herman, M.A., Peroni, O.D., Villoria, J., Schön, M.R., Abumrad, N.A., Blüher, M., Klein, S., and Kahn, B.B. (2012). A novel ChREBP isoform in adipose tissue regulates systemic glucose metabolism. Nature *484*, 333–338.

Hirasawa, A., Tsumaya, K., Awaji, T., Katsuma, S., Adachi, T., Yamada, M., Sugimoto, Y., Miyazaki, S., and Tsujimoto, G. (2005). Free fatty acids regulate gut incretin glucagon-like peptide-1 secretion through GPR120. Nat. Med. *11*, 90–94.

Hu, F.B. (2011). Globalization of diabetes: the role of diet, lifestyle, and genes. Diabetes Care *34*, 1249–1257.

Ichimura, A., Hirasawa, A., Poulain-Godefroy, O., Bonnefond, A., Hara, T., Yengo, L., Kimura, I., Leloire, A., Liu, N., Iida, K., et al. (2012). Dysfunction of lipid sensor GPR120 leads to obesity in both mouse and human. Nature *483*, 350–354.

Iizuka, K., Bruick, R.K., Liang, G., Horton, J.D., and Uyeda, K. (2004). Deficiency of carbohydrate response element-binding protein (ChREBP) reduces lipogenesis as well as glycolysis. Proc. Natl. Acad. Sci. USA *101*, 7281–7286.

Lumeng, C.N., and Saltiel, A.R. (2011). Inflammatory links between obesity and metabolic disease. J. Clin. Invest. *121*, 2111–2117.

Ma, L., Tsatsos, N.G., and Towle, H.C. (2005). Direct role of ChREBP.Mlx in regulating hepatic glucose-responsive genes. J. Biol. Chem. *280*, 12019–12027.

Mo, X.L., Wei, H.K., Peng, J., and Tao, Y.X. (2013). Free fatty acid receptor GPR120 and pathogenesis of obesity and type 2 diabetes mellitus. Prog. Mol. Biol. Transl. Sci. *114*, 251–276.

Moe, M.K., Strøm, M.B., Jensen, E., and Claeys, M. (2004). Negative electrospray ionization low-energy tandem mass spectrometry of hydroxylated fatty acids: a mechanistic study. Rapid Commun. Mass Spectrom. *18*, 1731–1740.

Moraes-Vieira, P.M., Yore, M.M., Dwyer, P.M., Syed, I., Aryal, P., and Kahn, B.B. (2014). RBP4 activates antigen-presenting cells, leading to adipose tissue inflammation and systemic insulin resistance. Cell Metab. *19*, 512–526.

Norseen, J., Hosooka, T., Hammarstedt, A., Yore, M.M., Kant, S., Aryal, P., Kiernan, U.A., Phillips, D.A., Maruyama, H., Kraus, B.J., et al. (2012). Retinol-binding protein 4 inhibits insulin signaling in adipocytes by inducing proinflammatory cytokines in macrophages through a c-Jun N-terminal kinase- and toll-like receptor 4-dependent and retinol-independent mechanism. Mol. Cell. Biol. *32*, 2010–2019.

Oh, D.Y., Talukdar, S., Bae, E.J., Imamura, T., Morinaga, H., Fan, W., Li, P., Lu, W.J., Watkins, S.M., and Olefsky, J.M. (2010). GPR120 is an omega-3 fatty acid receptor mediating potent anti-inflammatory and insulin-sensitizing effects. Cell *142*, 687–698.

Oh, Y., Walenta, E., Akiyama, T.E., Lagakos, W.S., Lackey, D., Pessentheiner, A.R., Sasik, R., Hah, N., Chi, T.J., Cox, J.M., et al. (2014). A Gpr120-selective agonist improves insulin resistance and chronic inflammation in obese mice. Nat. Med. *20*, 942–947.

Olefsky, J.M., and Glass, C.K. (2010). Macrophages, inflammation, and insulin resistance. Annu. Rev. Physiol. *72*, 219–246.

Rhee, E.P., Cheng, S., Larson, M.G., Walford, G.A., Lewis, G.D., McCabe, E., Yang, E., Farrell, L., Fox, C.S., O'Donnell, C.J., et al. (2011). Lipid profiling identifies a triacylglycerol signature of insulin resistance and improves diabetes prediction in humans. J. Clin. Invest. *121*, 1402–1411.

Risérus, U., Willett, W.C., and Hu, F.B. (2009). Dietary fats and prevention of type 2 diabetes. Prog. Lipid Res. *48*, 44–51.

Roberts, R., Hodson, L., Dennis, A.L., Neville, M.J., Humphreys, S.M., Harnden, K.E., Micklem, K.J., and Frayn, K.N. (2009). Markers of de novo lipogenesis in adipose tissue: associations with small adipocytes and insulin sensitivity in humans. Diabetologia *52*, 882–890.

Saghatelian, A., Trauger, S.A., Want, E.J., Hawkins, E.G., Siuzdak, G., and Cravatt, B.F. (2004). Assignment of endogenous substrates to enzymes by global metabolite profiling. Biochemistry *43*, 14332–14339.

Shepherd, P.R., and Kahn, B.B. (1999). Glucose transporters and insulin action—implications for insulin resistance and diabetes mellitus. N. Engl. J. Med. *341*, 248–257.

Shepherd, P.R., Gnudi, L., Tozzo, E., Yang, H., Leach, F., and Kahn, B.B. (1993). Adipose cell hyperplasia and enhanced glucose disposal in transgenic mice overexpressing GLUT4 selectively in adipose tissue. J. Biol. Chem. *268*, 22243–22246.

Smith, C.A., O'Maille, G., Want, E.J., Qin, C., Trauger, S.A., Brandon, T.R., Custodio, D.E., Abagyan, R., and Siuzdak, G. (2005). METLIN: a metabolite mass spectral database. Ther. Drug Monit. *27*, 747–751.

Sud, M., Fahy, E., Cotter, D., Brown, A., Dennis, E.A., Glass, C.K., Merrill, A.H., Jr., Murphy, R.C., Raetz, C.R., Russell, D.W., and Subramaniam, S. (2007). LMSD: LIPID MAPS structure database. Nucleic Acids Res. *35* (Database issue), D527–D532.

Tozzo, E., Shepherd, P.R., Gnudi, L., and Kahn, B.B. (1995). Transgenic GLUT-4 overexpression in fat enhances glucose metabolism: preferential effect on fatty acid synthesis. Am. J. Physiol. *268*, E956–E964.

Virtanen, J.K., Mursu, J., Voutilainen, S., Uusitupa, M., and Tuomainen, T.P. (2014). Serum omega-3 polyunsaturated fatty acids and risk of incident type 2 diabetes in men: the Kuopio Ischemic Heart Disease Risk Factor study. Diabetes Care *37*, 189–196.

EXTENDED EXPERIMENTAL PROCEDURES

Materials and Reagents

All chemical reagents were purchased from Sigma-Aldrich (St. Louis, MO) unless otherwise stated. Hydroxystearic acid was purchased from Indofine Chemical Company, Inc. (Hillsborough, NJ). [$^{13}C_{16}$]-Palmitic acid was purchased from Cambridge Isotopes Laboratories, (Andover, MA). Organic solvents for chemical synthesis were purchased from EMD Millipore (Billerica, MA). Solvents for HPLC were purchased from EMD Millipore and solvents for LC-MS were from Honeywell Burdick & Jackson.

Culture and Differentiation of Cells

3T3-L1 fibroblasts were maintained in DMEM supplemented with 10% bovine calf serum, pen/strep and maintained at 37°C and 5% CO_2. For adipocyte differentiation, 3T3-L1 fibroblasts were grown to confluency in 48-well plates. Cells were maintained at confluency for 2 days after which differentiation was initiated by culturing cells in DMEM containing 10% fetal calf serum (FCS), 4 μg/ml bovine insulin, 0.25 μM dexamethasone, 0.5 mM IBMX and 2 μM Rosiglitazone. 3 days after differentiation initiation, the media was removed and replaced with DMEM supplemented with 10% FCS. Media was changed every 2 days until cells were used for experimental studies at 7–14 days postdifferentiation initiation. STC-1 enteroendocrine cells were maintained in DMEM supplemented with 10% FCS, pen/strep and maintained at 37°C and 5% CO_2.

GPR120 siRNA Knockdown in Adipocytes

3T3-L1 adipocytes grown in 10cm plates were trypsinized 8 days postdifferentiation initiation and transfected with control siRNA or three different GPR120 targeting siRNA's (TriFecta siRNA Kit, IDT) individually or in combination by nucleofection following the manufacturers' instructions (Lonza). Knockdown efficiencies of GPR120 targeting siRNA's were evaluated by q-PCR 48 hr posttransfection (Figure S4B). siRNA #1 showed >93% inhibition of GPR120 mRNA expression compared to control siRNA (Figure S4B) and, therefore, GPR120 siRNA #1 was used for the entire study. siRNA sequences and qPCR primers are listed in Table S4.

Quantitative PCR

RNA was extracted using Tri-Reagent (MRC) and cDNA was generated with random hexamers (Clontech). Quantitative real-time PCR was performed with the ABI Prism sequence detection system. Each sample was run in duplicate, and the quantity of GPR120 mRNA in each sample was normalized to mouse TATA-box binding protein (mTBP) mRNA levels. All primers were obtained from IDT DNA. qPCR primer sequences are listed in Table S4.

GLP1 Secretion from Enteroendocrine Cells

GLP1 secretion studies were performed as described previously (Hudson et al., 2013). Briefly, STC-1 cells were plated in poly-d-lysine coated 24-well plates 72 hr before assay initiation. Cells were washed three times with incubation buffer B (Hanks' balanced salt solution supplemented with 20 mM HEPES and 2.5 μM KR-62436 (DPP-IV inhibitor, to prevent hydrolysis of GLP1)). Cells were incubated in incubation buffer containing test compounds or DMSO (≤0.1%) control at 37°C for 1 hr. Cell supernatants were collected in microcentrifuge tubes and centrifuged to remove cellular debris and assayed for active-GLP1 concentration using an active-GLP1 ELISA kit (Millipore, Billerica, MA).

[^{3}H]Deoxy-Glucose Uptake in Adipocytes

Differentiated 3T3-L1 adipocytes (7–14 days postdifferentiation) were treated with test compounds 2 days or 6 days (chronic treatment) or for 30 min (acute treatment) with PAHSAs or vehicle (DMSO, ≤ 0.1%) control. For transport assays, cells were washed twice with serum-free DMEM and incubated in serum-free DMEM for 2–3 hr at 37°C. Cells were then washed 3 times with Krebs-Ringer-HEPES (KRH) buffer (50 mM HEPES pH 7.4, 137 mM NaCl, 1.25 mM $CaCl_2$, 4.7 mM KCl, 5.0 mM, 1.25 mM $MgSO_4$). Cells were incubated in KRH for 30 min then incubated in KRH containing test compounds or DMSO (≤0.1%) control ± insulin for 25 min before the addition of a [^{3}H]deoxy-glucose/2-deoxyglucose solution, yielding final assay concentrations of 1 μCi of [^{3}H]deoxy-glucose and 100 μM 2-deoxy-glucose. After 5 min the KRH buffer was removed immediately by aspiration. Cells were washed 3 times in ice-cold PBS to inhibit further glucose uptake and wash away unincorporated radiolabeled [^{3}H]deoxy-glucose. Cells were solubilized with 1% Triton X-100. [^{3}H] levels were measured by liquid scintillation counting and normalized to protein concentration.

Human Pancreatic Islets

Human islets from a nondiabetic, 48-year-old female donor (80% pure and 95% viable) and a nondiabetic 44-year-old male donor (85% pure & 95% viable) were obtained from Prodo Laboratories, Inc. (Irvine, CA). Islets were incubated for 1 day at 37°C in human islet media provided by Prodo laboratories before insulin secretion experiments were performed. See Table S3 for metabolic characteristics of human donors.

Quantitation of Glucose-Stimulated Insulin Secretion in Human Islets

GSIS was assessed as outlined previously (Kowluru et al., 2010). Briefly, human islets were cultured overnight in low serum (2.5%)— and low glucose (2.5 mM) human islet media. Following a 2 hr incubation in Krebs-Ringer Bicarbonate buffer (KRB) with 0.5% BSA

(pH 7.4), islets were stimulated with either low (2.5 mmol/l) or high (20 mmol/l) glucose in KRB buffer in the presence or absence of vehicle for 5-PAHSA (Methanol, 0.25%) or 5-PAHSA (20 μM) for 45 min at 37°C. At the end of the incubation, media was collected and insulin released into the medium was quantitated by ELISA (Alpco).

GPR120 Activity Assay

GPR120 activity assays were performed using DiscoverRx assay kit (PathHunter eXpress GPR120L (Long Isoform) CHO-K1 β-Arrestin GPCR Assay (Part # 93-0366E2CP0M)) as per manufacturer's instructions.

Generation of Bone-Marrow-Derived Dendritic Cells and Treatment with PAHSAs

Mouse bone marrow cells were flushed from the femurs and tibiae of 8- to 12-week-old C57BL6/J male mice on a chow diet. Red blood cells were lysed with RBC lysis buffer (Biolegend), and the cells were plated in 6 wells flat bottom plate at a density of $1.0x10^6$ cells/ml in RPMI1640 (GIBCO) containing 10% FBS and supplemented with essential amino acids, pyruvate, glutamine, vitamins, β-mercaptoethanol and antibiotics (GIBCO). GM-CSF (R&D) at a concentration of 20 ng/ml was used for BMDC differentiation. The medium was replaced on day 4, and the cells were harvested on day 6 to obtain immature DC (nonactivated iDC). To obtain activated DC (mDC), LPS was added and the cells were cultured for an additional 24 hr. LPS was used at a final concentration of 100 ng/ml. 9-PAHSA was added 10 min prior to LPS treatment at a final concentration from 2 to 80 μM. Palmitic acid and oleic acid or vehicle (ethanol) control were added 10 min prior to LPS treatment at a final concentration of 40 μM. DMSO (≤0.2%) was added as a vehicle control for 9-PAHSA in experiments where indicated. Cytokines (Il-12p70, IL-1β, IL-6, and TNF-α) secreted into the media were measured by ELISA according to the manufacturers' instructions (Biolegend).

Animal Studies and Measurement of Metabolic Parameters

Female AG4OX mice and WT littermate controls (FVB background) were described previously (Herman et al., 2012; Shepherd et al., 1993). ChREBP-KO, ChREBP-KO/AG4OX and control females, described previously (Herman et al., 2012) were used at 16- to 18-week-old. Wild-type female FVB mice were also used for studies of FAHFA tissue distribution and the effects of fasting and HFD on FAHFA levels. For measurement of FAHFAs in serum and tissues of chow- and HFD-fed mice, C57BL6/J male mice were maintained on chow (Lab Diet, 5008) or HFD (Harlan Teklad, 93075) for 9 weeks. Animals were euthanized by decapitation and tissues were dissected, flash frozen in liquid nitrogen, and stored at −80°C. For metabolic studies (OGTT and glycemia with food removal), male C57BL6/J mice were fed on either chow (Lab Diet, 5008) or HFD (Harlan Teklad, 93075) for 42–52 weeks. Oral glucose tolerance tests (OGTT) were performed in awake mice after 5 hr food removal. At 4.5 hr after food removal (0.5 hr before initiation of the OGTT) mice were gavaged with 30 mg/kg (chow) or 45 mg/kg (HFD) 9-PAHSA, 5-PAHSA or an equivalent volume of vehicle (50% PEG400, 0.5% Tween-80, 49.5% H_2O). Mice received 1 g/Kg glucose by gavage 30 min after PAHSA or vehicle administration and glycemia was monitored over a 2 hr period. In OGTT studies with 5-PAHSA in chow-fed 45 week old male mice (Figure 5C), mice were bled 5 min postglucose gavage from the tail vein using heparin coated capillary tubes and blood was transferred into tubes containing KR-62436 (DPP-IV inhibitor, 2.5 μM final conc.) and serum insulin and total GLP-1 were measured by ELISA (insulin; Crystal Chem Inc., GLP-1; Millipore). In studies elucidating 9- and 5-PAHSA effects on ambient glycemia, HFD-fed mice were fasted for 2.5 hr and gavaged with either 5- or 9-PAHSA (45 mg/kg) or vehicle (50% PEG400, 0.5% Tween 80, 49.5% H_2O). Glycemia was measured before the gavage (time 0) and 150 min (5-PAHSA) or 180 min (9-PAHSA) postgavage. Mice were bled from the tail vein using heparin coated capillary tubes and serum insulin was measured by ELISA (Crystal Chem Inc.). All animals were kept on a 14 hr light, 10 hr dark schedule (no changes for daylight savings) at an ambient temperature between 72 and 74°F and fed *ad libitum* unless specified otherwise. All mice were housed in a barrier facility in individually ventilated cages. Male mice were housed individually. Female mice were housed 2–3 per cage. All animal care and use procedures were in strict accordance with, and approved by the Institutional Animal Care and Use Committee at Beth Israel Deaconess Medical Center, Boston, MA.

Human Samples

Thirteen nondiabetic subjects (9F/4M) with varying degrees of insulin sensitivity and BMI were recruited through advertisements in local media. Individuals diagnosed with diabetes or taking any chronic medication were excluded from participation. Height, weight and waist circumference were measured with conventional methods, BMI was calculated as kg body weight divided by height (m) squared. Fasting blood samples were drawn after an overnight fast. Circulating free fatty acid and triglyceride levels were determined by standard methods in the accredited central hospital laboratory using Wako kits (Nordic Biolabs, Täby, Sweden). To evaluate insulin sensitivity a hyperinsulinaemic-euglycaemic clamp was performed for 120 min with an insulin infusion rate of 40 mU/m^2 per min, essentially as described (DeFronzo et al., 1979; Laakso et al., 2008) Blood glucose was clamped at 5 mmol/l by infusion of 20% glucose at various rates according to the blood glucose measurements performed at 5 min intervals. The mean amount of glucose infused during the last hour was used to calculate the rate of whole-body glucose uptake and expressed per Kg lean body mass (LBM). Fat mass and LBM were calculated from bioimpedance analysis (Laakso et al., 2008). SQ WAT biopsies were obtained from the peri-umbilical, abdominal region after an overnight fast and snap frozen in liquid nitrogen. The study was approved by the local Ethical Committees at the Sahlgrenska Academy at the University of Gothenburg and performed in agreement with the Declaration of Helsinki. All subjects received written information and gave written consent to participate. See Table S2 for metabolic parameters of human participants.

9-PAHSA Biosynthetic Activity Assay

Fresh Liver and PG-WAT tissue was Dounce homogenized in buffer A (10 mM Tris-HCL pH 7.4, 250 mM Sucrose containing protease inhibiters [Roche]). Lysates were centrifuged at 1,200 g to remove incompletely lysed cells and debris. Lysates were then adjusted to 1 mg/ml protein and 100 μl was incubated with 100 μM palmitoyl-CoA and 100 μM 9-hydroxy stearic acid (PAHSA substrates) for 2 hr at 37°C. Control samples were heat denatured by boiling for 10 min prior to incubation with PAHSA substrates. After 2 hr the reaction was stopped by the addition of 300 μl cold buffer A followed by 400 μl of methanol and 800 μl of chloroform. Samples were vortexed and centrifuged at 1,200 g for 5 min. The bottom organic layer was transferred to a new glass vial and dried under a stream of nitrogen. 9-PAHSA levels were measured by LC-MS.

FAHFA Synthesis In Vivo

Two hours postfood removal C57BL6/J mice were gavaged with 25 mg/Kg of 9-hydroxy heptadecanoic acid or vehicle (50% PEG-400, 0.5% Tween-80, 49.5% H_20) control. Three hours later mice were sacrificed by decapitation and serum was collected. Serum lipids were extracted and palmitic-acid-9-hydroxy-heptadecanoic-acid (9-PAHHA) levels were measured by LC-MS.

Anti-Inflammatory Effects of 9-PAHSA In Vivo

Male C57BL6/J mice were fed on either chow (Lab Diet, 5008) or HFD (Harlan Teklad, 93075) for 42–52 weeks. Mice were gavaged once a day for 3 days with 30 mg/kg (chow) or 45 mg/kg (HFD) of 9-PAHSA or an equivalent volume of vehicle (50% PEG400, 0.5% Tween-80, 49.5% H_2O). On the fourth day mice were euthanized by decapitation and perigonadal stromal vascular (SVF) fraction obtained as described (Moraes-Vieira et al., 2014). SVF cells were cultured for 5 hr with ionomycin, PMA and brefendin at 37°C and the intracellular cytokine content measured as previously described (Moraes-Vieira et al., 2014).

Data Analysis

All values are given as mean ± SEM. Differences between groups were assessed using unpaired two-tailed Student's t tests and/or ANOVA with Fisher's LSD multiple comparisons as specified in figure legends. Correlations were determined by linear regression analysis yielding "r" and "p" values. All statistical analyses were performed with GraphPad Prism 5.0.

Lipid Extraction from Serum and Tissues

Lipid extraction was performed based on known protocol (Bligh and Dyer, 1959; Saghatelian et al., 2004). Murine tissues (60–150 mg), human fat biopsy (50–70 mg) were Dounce homogenized on ice for 40 strokes in a mixture of 1.5 ml: 1.5 ml: 3 ml citric acid buffer (100 mM trisodium citrate, 1 M NaCl, pH 3.6): methanol: chloroform. ^{13}C-9-PAHSA standard (0.5–5 pmol per sample depending on tissue type) was added to chloroform prior to extraction. The resulting mixture was centrifuged at 2,200 g, 6 min, 4°C to separate organic and aqueous phases, and the organic phase containing extracted lipids was removed with a Pasteur pipette, dried under a gentle stream of Nitrogen and stored at −80°C prior to solid phase extraction (SPE). Lipids were extracted from mouse serum (100 to 200 μl) and human serum (300 μl) using similar protocol, Citric acid buffer or PBS was added to serum such that the final volume was 1 ml for mouse serum and 1.5 ml for human serum, followed by addition of methanol and chloroform to maintain an aqueous: methanol: chloroform ratio of 1:1:2. The resulting mixture was shaken for 30 s by hand, vortexed for 15 s and then centrifuged to separate organic and aqueous phases. Organic phase containing lipids was removed, dried and stored following same method as tissues.

Solid Phase Extraction for FAHFA Enrichment

SPE was performed at room temperature via gravity flow. SPE cartridge (500 mg silica, 6 ml, Thermo Scientific, 60108-411) was conditioned with 15 ml hexane. Extracted lipids (reconstituted in 200 μl chloroform) were loaded onto column. Vial containing lipids was washed with an additional 100 μl chloroform and the wash also loaded onto the column. Neutral lipids were eluted with 16 ml 5% ethyl acetate in hexane, followed by elution of FAHFAs with 16 ml ethyl acetate. FAHFA fraction was dried under nitrogen and stored at −80 °C prior to LC-MS.

Mass Spectrometry

FAHFAs were measured on an Agilent 6410 Triple Quad LC/MS instrument via Multiple Reaction Monitoring (MRM) in negative ionization mode. A Luna C18(2) (Phenomenox, 00G-4251-B0) column (3 μm, 100 Å, 250 × 2.0 mm) was used with an in-line filter (Phenomenex, AF0-8497). The solvent was 93:7 methanol:water with 5 mM ammonium acetate (Aldrich, 372331) and 0.01% ammonium hydroxide (Sigma-Aldrich, 338818), and distinct PAHSA species were resolved via isocratic flow at 0.2 ml/min for 120 min. Each extracted and fractionated sample was reconstituted in 25 μl methanol and 10 μl was injected for analysis. Transitions for endogenous PAHSAs were m/z 537.5 → m/z 255.2 (CE = 30 V), m/z 537.5 → m/z 281.2 (CE = 25 V) and m/z 537.5 → m/z 299.3 (CE = 23 V), and transition for ^{13}C-9-PAHSA was m/z 553.5 → m/z 271.3 (CE = 30 V). Fragmentor voltage and dwell time were 205 V and 300 ms, respectively, for each transition. Skimmer voltage was 15 V and ΔEMV was 400 V. MS1 resolution was set to wide and MS2 resolution to unit. Capillary voltage was 4.0 kV, drying gas temperature was 350°C, drying gas flow rate was 8 L min^{-1} and nebulizer pressure was 35 psi. Identical gradient and instrument parameters were used for detection of all additional FAHFAs with the exception of dwell time, which was reduced to 30 ms to accommodate additional transitions. All FAHFA transitions are listed in Table S1.

Targeted LC-MS Quantitation of PAHSA Biosynthetic Reactions Performed In Vivo and In Vitro

Samples for analysis of 9-PAHSA biosynthetic activity were dissolved in 50 μl methanol. The LC-MS method was slightly modified from the targeted FAHFA method. The column was changed to an ACQUITY UPLC BEH C18 column (1.7 μm, 130Å, 2.1 mm X 100 mm) and maintained at 40°C during separation. The elution time was shortened to 40 min. The injection volume is 10 μl. For analysis of 9-PAHHA synthesis in vivo, similar 40 min gradient LC-MS method was employed, but the corresponding MRM transitions used for 9-PAHHA were m/z 523.5 → m/z 255.2, m/z 523.5 → m/z 267.2 and m/z 523.5 → m/z 285.3.

Lipidomics of WT and AG4OX SQ WAT

A Gemini C18 reversed phase column (5 μm, 4.6 × 50 mm, Phenomonex) and a C18 reversed phase guard column (3.5 μm, 2 × 20 mm, Western Analytical) were used for LC-MS analysis in negative mode. In positive mode, a Luna C5 reversed phase column (5 μm, 4.6 × 50 mm, Phenomonex) was used together with a C4 reversed phase guard column (3.5 μm, 2 × 20 mm, Western Analytical). 30 μl of each sample was injected using an autosampler. Mobile phase A consisted of a 95:5 water:methanol mixture and mobile phase B consisted of 60:35:5, 2-propanol:methanol:water. In negative mode 0.1% ammonium hydroxide was added to the mobile phases and in positive mode 0.1% formic acid plus 5 mM ammonium formate were added. An Agilent 1200 series binary pump method was set to a flow rate of 0.1 ml/min for the first 5 min followed by 0.4 ml/min for the remainder of the gradient. At 5 min, concomitant with the increase in flow rate, the gradient was increased from 0% B to 20% B. The gradient increased linearly to 100% B at 45 min, followed by an 8 min wash at 0.5 ml/min with 100% B before re-equilibrating the column with 0% B for 7 min. MS analysis was performed using an Agilent 6220 ESI-TOF fitted with an electrospray ionization (ESI) source. The capillary voltage was set to 3,500 kV and the fragmentor voltage to 100 V. The drying gas temperature was set to 350°C at a flow rate of 10 l/min with a nebulizer pressure set to 45 psi. Untargeted data were collected using a mass-to-charge range of *m/z* 100–1,500.

MS Data Analysis

Data analysis with XCMS was used to identify changing metabolites between samples. Raw data files from the TOF-MS were converted to mzXML files using the program mzStar for subsequent XCMS analysis. Samples were compared (i.e., AG4OX versus WT) and differences were ranked according to statistical significance as calculated by an unpaired Student's t test. The data were then filtered based on a peak size (>5 × 10^4 counts) and statistical significance (p value < 0.05) prior to visual inspection of the remaining ions to ensure that the differences identified by XCMS were reflected in the raw data. Peak areas were normalized to the frozen wet mass of the extracted tissues and these corrected peak areas were used to calculate relative changes. For the volcano plot, data were obtained from the 60 min profiling analysis in negative mode and the data were filtered based on retention time range (10–50 min) and abundance (>1 × 10^5 counts).

Purification of PAHSAs from Mouse Tissue to Identify the Predominant PAHSA Isomer in SQ WAT by Tandem MS

PAHSA in microgram quantities was obtained by purification from WAT (0.75 g) harvested from AG4OX mice. After homogenizing the tissue and extracting the homogenate with chloroform-methanol, triglycerides were removed from the lipid extract (0.6 g) by flash chromatography on an alumina column. Neutral lipids were eluted with 20% ethyl acetate in hexanes, and the remaining lipids were eluted with 2% acetic acid in ethyl acetate. The fractions were combined and the solvent was removed *in vacuo*. The oily residue was then purified by preparative reversed phase HPLC (Shimazu). The preparative column dimensions were 20 × 150 mm, the particle size was 10 μm, and the stationary phase was C18. Buffer A was 100% water and Buffer B was 100% methanol, both containing 10 mM ammonium acetate. The flow rate was 8 ml/min and the solvent composition started at 60% B, where it was held for 5 min. The composition was increased to 100% B over 60 min, after which the column was washed with 100% B for 20 min. The PAHSA-containing fractions, assessed by QQQ-MS in MRM mode, were combined. PAHSA eluted in minutes 68–70 on this gradient, and the methanol-water eluate was evaporated under a nitrogen gas stream, leaving an oily residue (6.8 mg). Analysis of the residue by TOF-MS demonstrated that PAHSA was the dominant component of the mixture and the absence of hydroxystearic acid was verified. For structural characterization by MS/MS, the PAHSA residue was reconstituted in chloroform for injection on the triple quadrupole mass spectrometer.

Structural Analysis by Q-TOF Mass Spectrometry

Structural characterization of the FAHFAs by MS/MS was initially carried out on an Agilent 6510 quadrupole-time of flight mass spectrometer. The chromatography setup was similar to the above conditions, but the runtime was lowered to 45 min by shortening the linear gradient from 45 min to 30 min. Fragmentation spectra of PAHSA were initially obtained using a collision energy of 20 V, but fragmentation of the 12-PAHSA standard to generate diagnostic fragment ions was performed at 50 V. The target mass was *m/z* 537.488, the MS scan range was *m/z* 100–1,000 and the MS2 scan range was *m/z* 50–1,000 with an acquisition time of 1,000 ms. The Q-TOF-MS was fitted with an ESI source, and the capillary voltage was set to 3,500 V, the fragmentor voltage was set to 100 V, and the skimmer voltage was set to 60 V. The drying gas temperature was set to 350°C at a flow rate of 10 l/min with a nebulizer pressure set to 45 psi.

SUPPLEMENTAL REFERENCES

DeFronzo, R., Tobin, J., and Andres, R. (1979). Glucose clamp technique: a method for quantifying insulin secretion and resistance. Am. J. Physiol. *237*, E214–E223.

Hudson, B.D., Shimpukade, B., Mackenzie, A.E., Butcher, A.J., Pediani, J.D., Christiansen, E., Heathcote, H., Tobin, A.B., Ulven, T., and Milligan, G. (2013). The pharmacology of TUG-891, a potent and selective agonist of the free fatty acid receptor 4 (FFA4/GPR120), demonstrates both potential opportunity and possible challenges to therapeutic agonism. Mol. Pharmacol. *84*, 710–725.

Kowluru, A., Veluthakal, R., Rhodes, C.J., Kamath, V., Syed, I., and Koch, B.J. (2010). Protein farnesylation-dependent Raf/extracellular signal-related kinase signaling links to cytoskeletal remodeling to facilitate glucose-induced insulin secretion in pancreatic beta-cells. Diabetes *59*, 967–977.

Laakso, M., Zilinskaite, J., Hansen, T., Boesgaard, T.W., Vänttinen, M., Stancáková, A., Jansson, P.A., Pellmé, F., Holst, J.J., Kuulasmaa, T., et al.; EUGENE2 Consortium (2008). Insulin sensitivity, insulin release and glucagon-like peptide-1 levels in persons with impaired fasting glucose and/or impaired glucose tolerance in the EUGENE2 study. Diabetologia *51*, 502–511.

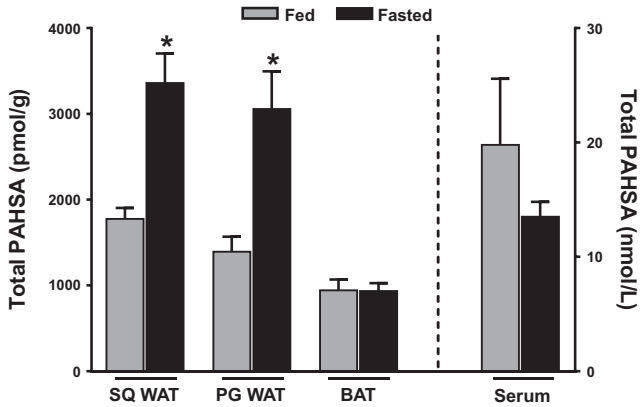

Figure S1. Quantification of PAHSA Levels in AG4OX Mouse Adipose Tissue Depots and Serum in Fed and Fasted States, Related to Figure 2D

Total PAHSA levels in adipose tissue and serum of female AG4OX mice in fed or fasted (16 hr) states. n = 3–5 per group, *$p < 0.05$ compared to fed (t test). Data are means ± SEM. SQ: subcutaneous, PG: perigonadal, WAT: white adipose tissue, BAT: brown adipose tissue.

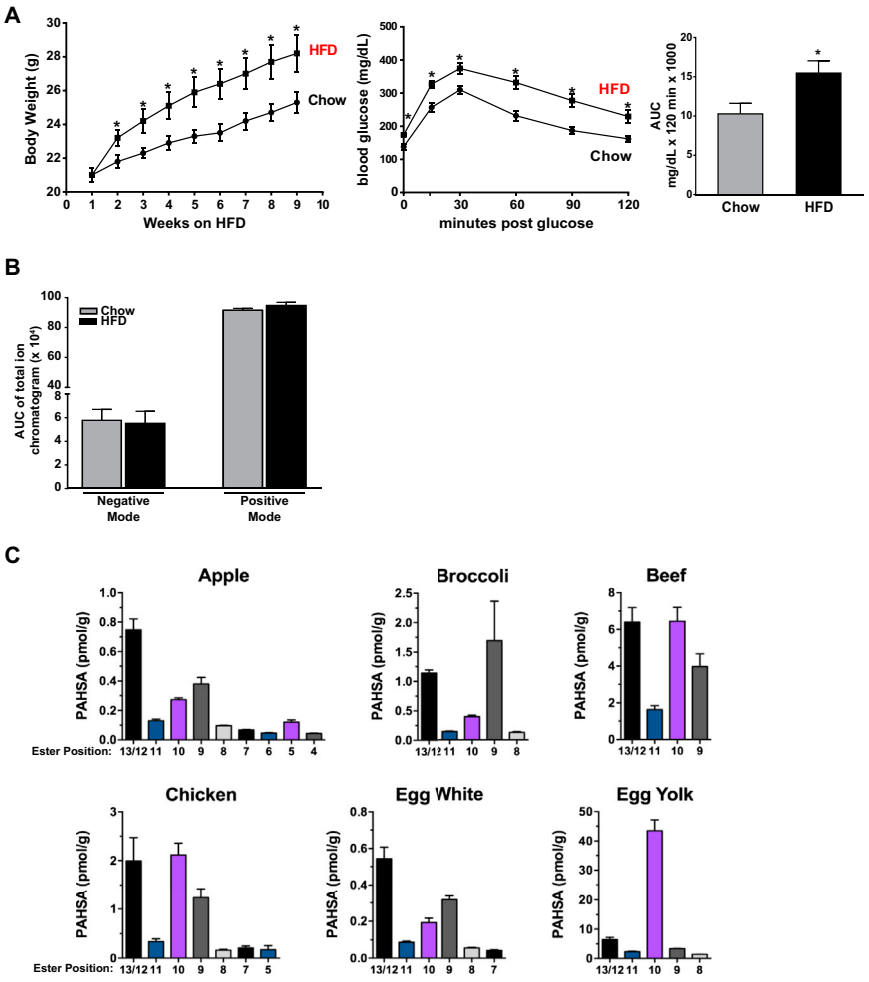

Figure S2. Characterization of Body Weight, Glucose Tolerance, and Adipose Tissue Total Lipid Ion Content in High Fat Diet-Fed Mice, and PAHSA Isomers in Common Human Foods, Related to Figure 3

(A) Growth curve and oral glucose tolerance test in chow- and HFD-fed mice. Body weight (grams) of female FVB mice fed chow or HFD for 9 weeks (left panel). Oral glucose tolerance test 6 hr after food removal in female FVB mice fed chow or HFD (middle left panel). Area under the OGTT curve (AUC) measured from time 0 to 120 min (right panel). Data are presented as mean ± SEM, t-test *$p < 0.05$, n = 9–12 mice per group. Tissues from four chow and three HFD mice were used for lipid measurements in Figure 3A.

(B) Total ion signal in subcutaneous adipose tissue from female FVB mice on chow or high-fat diet for 9 weeks. Lipids were extracted from subcutaneous adipose tissue and subjected to untargeted lipidomic analysis by LC-MS. The total negative and positive ion chromatograms of subcutaneous adipose tissue from chow- or HFD-fed mice (n = 3, 17–18 weeks old) were integrated.

(C) PAHSA isomer levels in human foods. Lipids were extracted from common human foods and PAHSA isomers were quantified using LC-MS. Data are means ± SEM, n = 3 per group.

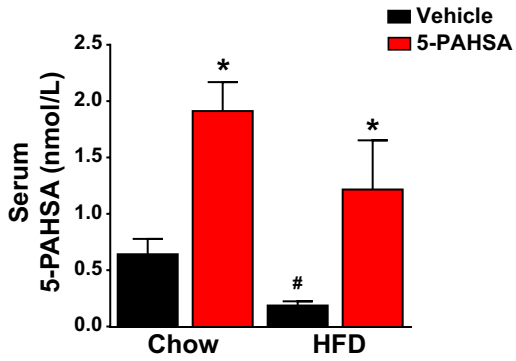

Figure S3. Serum 5-PAHSA Levels after Oral Administration of Synthesized 5-PAHSA, Related to Figures 5A–5C

Three hours after food removal, C57BL6/J male mice (46–48 weeks old) were gavaged with 5-PAHSA (30 mg/kg chow or 45 mg/kg HFD-fed). 5 hr postgavage, blood was collected via tail vein and serum 5-PAHSA levels were determined by LC-MS. Data are expressed as mean ± SEM, t-test *$p < 0.05$ versus vehicle-treated mice on the same diet; and #$p < 0.05$ versus chow-fed vehicle-treated mice. n = 3 mice per group.

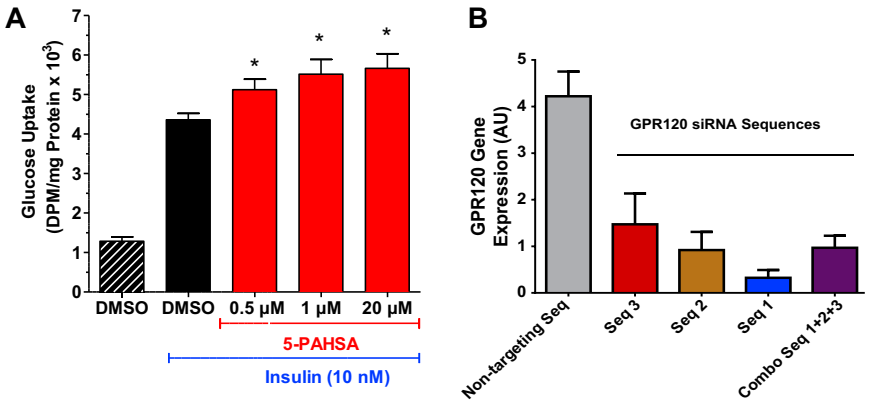

Figure S4. Dose-Dependent Enhancement of Insulin-Stimulated Glucose Uptake by 5-PAHSA and Confirmation of GPR120 Knockdown in Adipocytes, Related to Figure 6

(A) Insulin-stimulated glucose transport in 3T3-L1 adipocytes treated with 5-PAHSA at the concentrations indicated or vehicle (DMSO, $\leq$ 0.1%) control for 48 hr. Data are means ± SEM, n = 3 per group, t-test *p < 0.05 compared to DMSO + Insulin.

(B) Validation of GPR120 knockdown in differentiated 3T3-L1 adipocytes. 3T3-L1 adipocytes (Day 8 postdifferentiation) were transfected with nontargeting (control) siRNA or three individual GPR120 targeting siRNAs individually or in combination. 48 hr posttransfection GPR120 mRNA levels were measured by qPCR and normalized to TBP mRNA levels. Data are means ± SEM, n = 3 wells per condition. Studies in Figure 6 were performed with sequence 1.

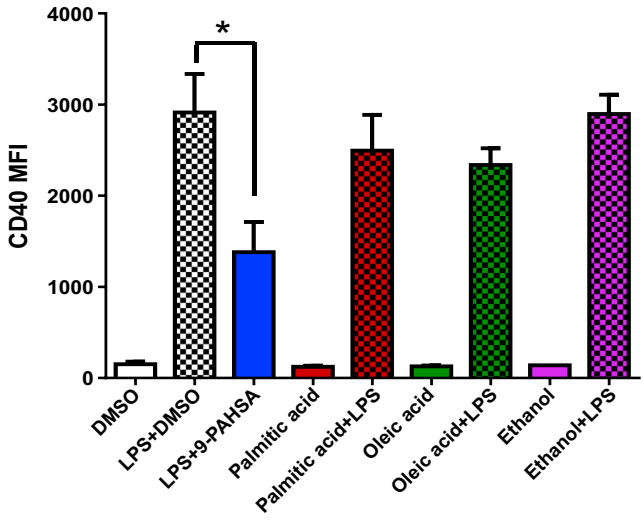

Figure S5. CD40 Induction by LPS in Bone-Marrow-Derived Dendritic Cells Is Inhibited by Pretreatment with 9-PAHSA, Related to Figure 7

Addition of LPS (100 ng/ml) induces CD40 levels and this induction is blunted by pretreatment with 9-PAHSA (40 μM) but not the addition of palmitic or oleic acid (20 μM). Data are expressed as means ± SEM. n = 4–5 wells per group. *$p < 0.05$ versus LPS + DMSO (≤0.2%). 20 μM 9-PAHSA shows similar effects (See Figure 7B).